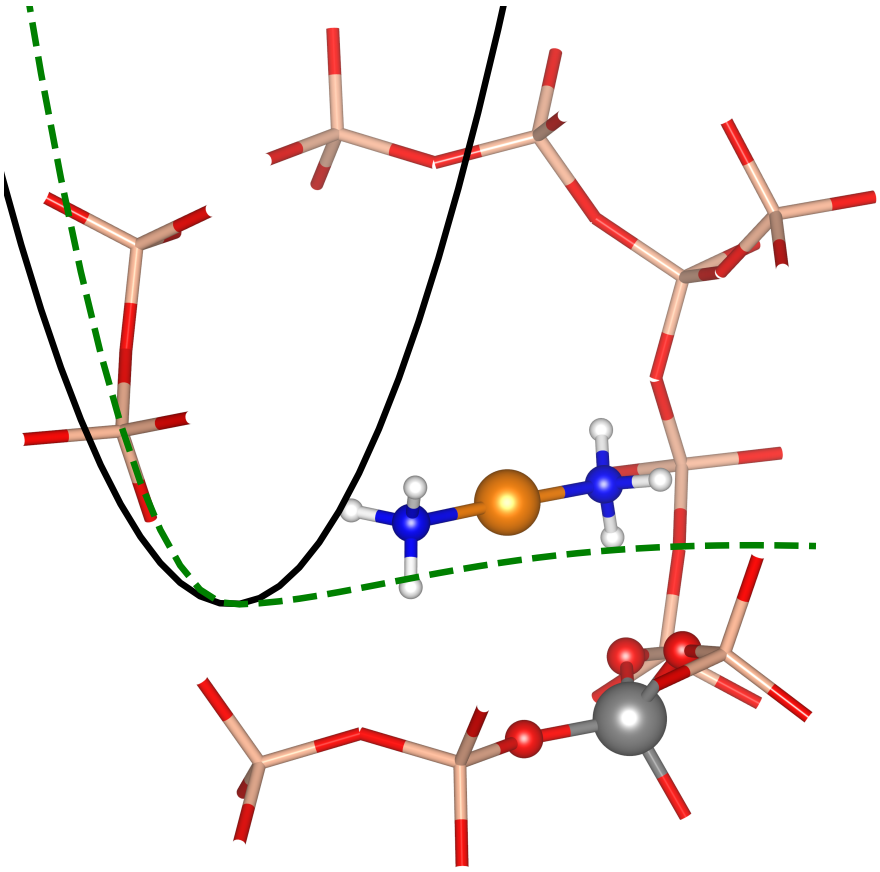

Entropies of weakly adsorbed molecules beyond the harmonic approximation

Master's thesis in Physics

OLOF CRONQUIST

DEPARTMENT OF PHYSICS
DIVISION OF CHEMICAL PHYSICS
CHALMERS UNIVERSITY OF TECHNOLOGY
Gothenburg, Sweden 2023
www.chalmers.se

Master's thesis 2023

Entropies of weakly adsorbed molecules beyond the harmonic approximation

OLOF CRONQUIST

CHALMERS
UNIVERSITY OF TECHNOLOGY

Department of Physics
Division of Chemical Physics
Chalmers University of Technology
Gothenburg, Sweden 2023

Entropies of weakly adsorbed molecules beyond the harmonic approximation
OLOF CRONQUIST

© OLOF CRONQUIST, 2023.

Supervisor: Prof. Henrik Grönbeck, Department of Physics
Examiner: Prof. Henrik Grönbeck, Department of Physics

Master's Thesis 2023
Department of Physics
Division of Chemical Physics
Chalmers University of Technology
SE-412 96 Gothenburg
Telephone +46 31 772 1000

Cover: A fictitious figure of a $[Cu(NH_3)_2]^+$ molecule adsorbed in SSZ-13 zeolite, escaping the harmonic approximation.

Typeset in LaTeX
Printed by Chalmers Reproservice
Gothenburg, Sweden 2023

Entropies of weakly adsorbed molecules beyond the harmonic approximation
OLOF CRONQUIST
Department of Physics
Chalmers University of Technology

Abstract

Adsorption processes and reaction kinetics are described by the free energy. While the enthalpy contribution to the free energy can be evaluated with reasonable accuracy thanks to the developments of density functional theory (DFT), methods to accurately describe the entropy contributions are in many cases missing. One important example is adsorption in zeolites where some adsorbates are physisorbed, which is a state where the common harmonic approximation, as well as more sophisticated methods, can not accurately describe the entropy. Zeolites are crystalline microporous materials and have many applications, for example as catalysts. An important catalytic reaction over a zeolite material is selective catalytic reduction of NOx with ammonia as reducing agent (NH_3-SCR).

In this thesis, the entropy of species related to the NH_3-SCR reaction is explored using two different methods, namely Complete Potential Energy Sampling (CPES) and Thermodynamic Integration (TI). Both methods rely on potential energy surfaces that are obtained with DFT calculations. In CPES, the full multidimensional potential energy surface is sampled by, for example, metadynamics. In TI, the starting point is the harmonic reference system to which calculates anharmonic corrections to the free energy are evaluated. Successful implementation of each method was demonstrated by reproducing results from previous works. When applicable, entropies were compared to experimental data, where only CPES showed to be in good agreement. However, free energy is the primary result of TI and our results are in good agreement with experimental data for the free energy and it is uncertain whether the entropy extraction, underlying method, or simulation setup is the culprit of TI. The results presented in the thesis increase the general understanding of entropies of weakly adsorbed molecules and, in particular, the understanding of entropy changes along the NH_3-SCR reaction.

Keywords: entropy, free energy, adsorption, anharmonicity, van der Waals, zeolites, Complete Potential Energy Sampling, Thermodynamic Integration

Acknowledgements

I want to thank my supervisor and examiner Professor Henrik Grönbeck for giving me the opportunity to write this thesis and for the interesting discussions and your guidance during the project. And thank you for your patience.

I would also like to thank my friend and opponent Patrik for the nice coffee breaks and Martina for being my biggest supporter.

Olof Cronquist, Gothenburg, January 2023

List of Acronyms

Below is the list of acronyms that have been used throughout this thesis listed in alphabetical order:

AIMD	Ab initio molecular dynamics
CPES	complete potential energy sampling
DFT	density function theory
hMD	harmonic molecular dynamics
MD	molecular dynamics
RDF	radial distribution function
TI	thermodynamic integration

Contents

1

Introduction

Utilizing catalysis to enhance desired chemical reactions is important to our society, and understanding the underlying mechanisms of catalysis is desirable to be able to tune the materials properties of the catalysts. A promising group of catalysts is zeolites, a crystalline microporous material. Zeolites are used in heterogenous catalysis while having some properties of homogenous catalysts, so they have high efficiency and selectivity and are also easily separated from the reactants and products [13].

However, in comparison to a surface substrate, the description of the adsorbate state and the free energy of adsorption is more complicated because the adsorbed molecule is confined inside the three-dimensional cage-like framework structure of the zeolite substrate. When confined in a zeolite pore, some adsorbates are merely bound to the zeolite with weak van der Waals (vdW) interactions [1]. Those adsorbates have larger translationally and rotationally mobility than that of an adsorbate that is bound to a surface with a strong, chemical bond, i.e. a covalent or ionic bond. Thus, it is difficult to accurately determine the entropy, a quantity very much dependent on the freedom of the adsorbate. For example, it seems as the harmonic approximation that is often used, for some adsorbates fails to describe the entropy of a molecule in a zeolite [32].

Entropy is part of the free energy, which is the main descriptor of stability of states and phases and is required to explain, for example, reactions kinetics. Reaction kinetics explains which reactions that take place and at which rate the reaction occurs. In other words, accurate entropies are essential to model and describe the adsorption process. The influence of entropy is illustrated in fig. 1.1. Two phase diagrams are shown in which the adsorbed molecule keeps 30% and 60% of its gas phase translational and rotational entropy when adsorbed. The diagrams differ vastly, indicating the need for accurate entropies.

An application of zeolites is the Ammonia assisted selective catalytic reduction (NH_3−SCR) where NH_3, NO and O_2 are transformed to N_2 and H_2O. NH_3−SCR is, for example, used to control emissions from "lean burn" engines. The zeolite used as catalyst is the copper exchanged SSZ-13 (denoted Cu-CHA). Unfortunately, a side reaction of NH_3−SCR is the production of N_2O, a potent greenhouse gas [13]. We want to accurately understand the mechanisms of the reaction so that the zeolite material can be tuned to limit the production of this unwanted side product.

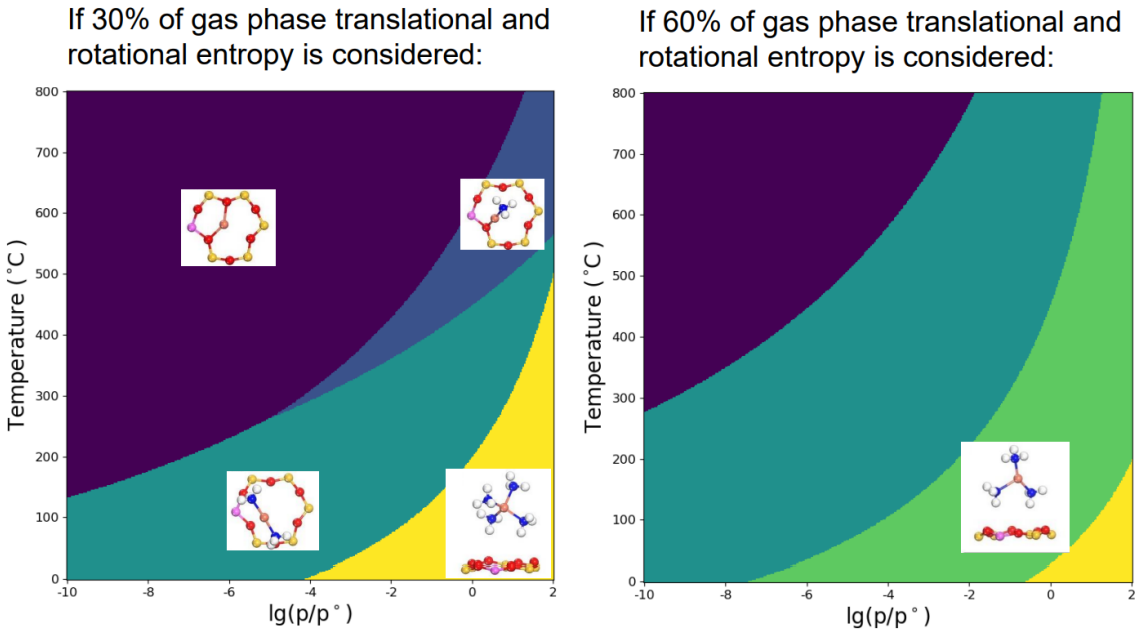

Figure 1.1: Phase diagrams illustrating the sensitivity on entropy. Adapted from [9].

1.1 Current methods to evaluate entropy

Various methods to calculate the entropy of adsorbates exist, ranging from simple to more advanced. As mentioned earlier, the harmonic approximation (HA) is a simple and common method to estimate the entropy, where translational and rotational degrees of freedom are approximated as vibrations [32]. Other approximations are the free translator (FT) and hindered translator (HT) approximations [33]. These are illustrated in fig. 1.2, along with the more sophisticated method Complete Potential Energy Sampling (CPES). With CPES, the full multidimensional potential energy surface is constructed, here in two dimensions, from which the entropy can be determined. A visualization of the models HA, FT, HT and CPES for CO adsorbed on a Pt surface is seen in fig. 1.3.

An additional method is Thermodynamic Integration (TI). The implementation of Thermodynamic Integration by Amsler et al. (2021) [1] utilizes translationally and rotationally invariant internal coordinates. The method starts from the harmonic approximation and calculates the harmonic free energy. Molecular dynamics simulations are in a second step used to evaluate anharmonic corrections to the free energy. Further, vibrational modes are also used by Galimberti and Sauer (2021) [21], where they find the vibrational density of states (VDOS) from molecular dynamic simulations and integrate the VDOS to gain more accurate vibrational free energies of adsorption.

A pragmatic approach by Feng (2021) [14], involves fitting a scaling factor to adsorption experimental data, in this case temperature programmed desorption, and

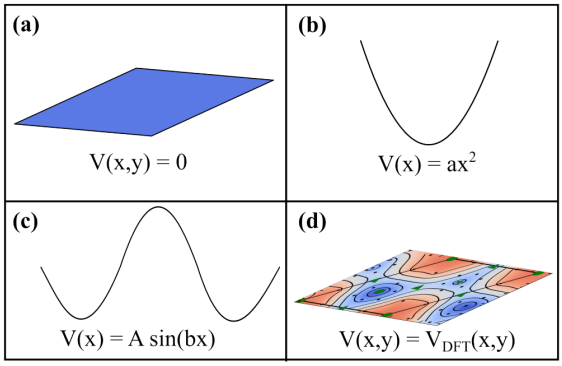

Figure 1.2: Schematic illustration of the potential energy landscape for translation in (a) the free translator model, (b) the harmonic approximation, (c) the hindered translator model, and (d) CPES. With permission from ref [31]. Copyright 2019 Mikkel Jørgensen.

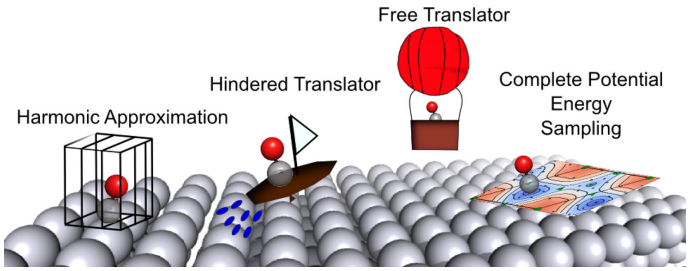

Figure 1.3: Illustration of different models the models HA, FT, HT and CPES used to calculate the adsorption entropy of CO adsorbed on a Pt surface. With permission from ref [33]. Copyright 2017 American Chemical Society.

scaling the gas phase entropy accordingly for all adsorbate states to get an estimate of the entropy.

1.2 Aim of thesis

In this thesis, emphasis is put on estimating adsorbate entropies where anharmonicity is accounted for with the more advanced methods CPES and TI. The aim is to implement these methods satisfactorily and evaluate their accuracy and suggest further improvements. Specifically, zeolites and molecules associated with the ammonia assisted selective catalytic reduction (NH_3−SCR) over Cu-SSZ-13 (Cu-CHA) will be considered. However, as the description of adsorbate entropies in zeolites is a general issue, understanding will affect a range of reactions such as, methane to methanol, and a range of selective transformations.

CPES specifically, builds upon the work of Jørgensen, Chen and Grönbeck (2018) [32] and Edenborg (2019) [12]. Where, in the first paper, CPES for zeolite systems in combination with sampling the PES with help of Monte Carlo sampling was introduced. In the second paper, molecular dynamics, and in particular metadynamics, were used to sample the local minima of PES. In this thesis, combining metadynam-

ics and CPES will be continued. While for TI, the aim is to successfully reproduce the results in the TI reference article [1], as well as implement the method for the more complex system $[Cu(NH_3)_2]^+$@CHA .

1.3 Scope

This thesis is limited to calculating the entropy for the selected systems N_2 and $[Cu(NH_3)_2]^+$ adsorbed in SSZ-13 with Si/Al ratio 11/1. Although, the primary result of TI is the free energy and is therefore also calculated. To demonstrate the implementation of the methods additional systems are also studied, that are reproduced from previous implementations. N_2 adsorbed in chabazite silicalite, N_2 @CHA$-SiO_2$, is also studied with CPES, and an HF molecule with TI.

2
Theory

In this chapter, the fundamentals of statistical physics and specifically the concept of entropy will be presented. The two methods investigated, CPES and TI, are introduced. Moreover, molecular dynamics (MD) which both methods use is introduced, as well as metadynamics (MTD) which is an extension of MD and is used in CPES. Furthermore, the theory behind density functional theory used for electronic structure calculations is briefly discussed.

2.1 Molecular dynamics

Molecular dynamics (MD) is a numerical tool to calculate the time evolution of the movement of atoms and molecules by solving the classical equations of motion. For example, equilibrium and transport properties can be simulated using MD [18]. In other words, one does "experiments" on a computer. With position $\boldsymbol{r}$, velocity $\boldsymbol{v}$ and acceleration $\boldsymbol{a}$ of an atom at time t and with an integration time step Δt, the most common integration scheme is the velocity Verlet algorithm, given by [18]

$$\begin{aligned} \boldsymbol{v}(t+\Delta t/2) &= \boldsymbol{v} + \frac{1}{2}\boldsymbol{a}(t)\Delta t \\ \boldsymbol{r}(t+\Delta t) &= \boldsymbol{r}(t) + \boldsymbol{v}(t+\Delta t)\Delta t \\ \boldsymbol{v}(t+\Delta t) &= \boldsymbol{v}(t+\Delta t/2) + \frac{1}{2}\boldsymbol{a}(t+\Delta t)\Delta t. \end{aligned} \tag{2.1}$$

The acceleration $\boldsymbol{a}(t) = \boldsymbol{F}/m$, where $\boldsymbol{F}$ is the force acting on the atom and m its mass. The forces can be given by some analytical functions, also known as force-fields. If the potential is $V(\boldsymbol{r})$, the force on an atom is given by $\boldsymbol{F} = -\frac{\partial V(\boldsymbol{r})}{\partial \boldsymbol{r}}$. The forces can also be determined quantum mechanically using density functional theory (DFT), described below in section 2.2. Molecular dynamics driven by forces from DFT is called ab initio MD (AIMD), while MD with potentials is called classical MD.

Often one is interested in doing the MD simulation at a specific temperature. The velocity Verlet algorithm above describes dynamics in the microcanonical ensemble (NVE), where the number of particles, volume and energy is kept constant. The concept of ensembles is discussed more thoroughly later in section 2.4. To control the temperature, the canonical ensemble (NVT) can be used, where the number of particles, volume and temperature are constant, and a so called thermostat is used for this

purpose. It is important to allow the temperature to stabilize, known as equilibration, and discard this data in the analysis. In this thesis, two thermostats are used, Andersen [2] and Nosé-Hoover [26, 27]. The Andersen thermostat is stochastic and models particles from a fictitious heat bath at a chosen temperature, that randomly collide with particles in the system. The hit particles immediately get assigned a new velocity from the Maxwell-Boltzmann distribution at the chosen temperature. The collision probability parameter must be set by the user [19]. Nosé-Hoover on the other hand is deterministic, where an additional coordinate in the Lagrangian and Hamiltonian is introduced, that is coupled to a heat bath. The coupling strength is a parameter [19].

2.2 Density function theory

The electronic structure of a system is within quantum mechanics described by the time independent many-body Schrödinger equation

$$\hat{H}\Psi = E\Psi \tag{2.2}$$

where $\hat{H}$ is the Hamiltonian of the system, E the eigenvalues and Ψ the eigenfunctions, also known as the wave function. To solve the Schrödinger equation for a system more complex than a hydrogen atom is practically very difficult, therefore various approximations are used to solve this many-body equation [47]. A first approximation is the Born-Oppenheimer approximation where the heavy nuclei are considered to be fixed while the low mass electrons move fast in the nuclei's electrostatic field. The electronic structure is left to be solved. However, the Schrödinger equation is still difficult to solve for more than one electron [47].

To get the actual DFT formalism, the work of Hohenberg, Kohn and Sham is required [25, 34]. In short, instead of solving for the wave function Ψ, the electron density can be used to calculate the electronic energy while preserving the many-body effects. Furthermore, the Kohn-Sham approach with one electron orbitals is introduced, where the density is [47]

$$n(\boldsymbol{r}) = \sum_i |\psi_i|^2 \tag{2.3}$$

and the energy is given by the functional

$$E[n] = T[n] + J[n] + V_{\text{ext}}[n] + V_{\text{xc}}[n]. \tag{2.4}$$

Here $T[n]$ is the kinetic energy of the non-interacting particles, $J[n]$ is the electron-electron Coloumb interaction, $V_{\text{ext}}[n]$ is the nuclei-electron potential energy and $V_{\text{xc}}[n]$ is the exchange-correlation energy. The first three terms are known and have explicit expressions, while the exchange-correlation term must be approximated. The equation to be solved is the Kohn-Sham equation, which includes the energy contributions just mentioned. The equation is solved self-consistently since the solution $n(\boldsymbol{r})$ is required to calculate the energy, which in turn is required to calculate the solution. The equation is therefore solved with an initial guess of $n(\boldsymbol{r})$ and the

solution is iterated in a self-consistent field (SCF) loop until a convergence criterion of the energy is met [47].

The exchange-correlation term $V_{\text{xc}}[n]$ is difficult to describe, and in this thesis, van der Waals interactions are of great importance and are incorporated in this term. As well as the description of highly localized electrons, in this thesis important for the copper complex $[\text{Cu}(\text{NH}_3)_2]^+$, is included in the exchange correlation term with a so called Hubbard term [13], which is further described in the method chapter.

2.3 Metadynamics

Metadynamics (MTD) is an MD technique to enhance the exploration of the free energy surface (FES) of some coordinate, or coordinates, of interest [39]. The coordinates of MTD are called collective variables (CV), denoted ξ, and might consist of combinations of primitive coordinates, such as interatomic distances, angles and cartesian coordinates. By continuously adding, on-the-fly, gaussian bias potentials to the FES of the CV during the MD simulation, local (and global) minima can be escaped and other unfavourable meta-stable states might be reached, that otherwise would be unvisited due to large energy barriers [7]. By adding bias potentials, the particle/atom/molecule can be seen as floating up from the bottom of its initial energy well, so after some time being able to move to another well.

In practice, MTD is implemented with a time dependent potential $V_{\text{bias}}(t, \xi)$, where t is time and ξ the CV, that is updated by adding a gaussian with a time increment t_G as the place of ξ at time it_G as follows [30]

$$V_{\text{bias}}(t, \xi) = h \sum_{i=1}^{t/t_G} \exp\left\{ -\frac{|\xi^{(t)} - \xi^{(it_G)}|^2}{2w^2} \right\}. \tag{2.5}$$

In other words, where ξ often visit, most gaussians are added. In eq. (2.5), h is the height and w the width of the gaussians. These parameters, as well as t_G can be changed during the MTD simulation. The bias potential $V_{\text{bias}}(t, \xi)$ is added to the Hamiltonian of the original, unbiased, system $\mathcal{H}(r, p)$, where r is position and p momentum. The resulting Hamiltonian for the MTD is then [30]

$$\mathcal{H}_{\text{MTD}}(r, p, t) = \mathcal{H}(r, p) + V_{\text{bias}}(t, \xi). \tag{2.6}$$

MTD is mostly used to construct a FES, where the free energy A is reached as $t \longrightarrow \infty$, $A(\xi) = -\lim_{t \longrightarrow \infty} V_{\text{bias}}(t, \xi) + C$, where C is a constant. To succeed with such MTD simulation, often meticulous care must be taken when choosing CV and the parameters t_g, h and w [7]. Adding too large gaussians too often will result in a FES where not all details are captured. Adding instead adding too small gaussians will require long simulation times. However, in this thesis the FES is not of interest, but the potential energy surface (PES). Therefore, it is not crucial to select the perfect parameters, since the PES is calculated separately from the added bias potential, but still is it desirable to sample the PES as efficiently as possible and also avoid missing local minima.

2.4 Statistical mechanics and entropy

Systems in nature are often too large and complex to analyze exactly in detail. Examples of such systems could be an ice cube, a magnet or a crowd of people. However, it is not feasible to solve for the behaviour of every atom in the ice cube, every electron in a magnet or every person in a crowd. Therefore, we use statistical mechanics to explain the macroscopic behaviour of large complex systems and model the microscopic complexities. In statistical mechanics, the behaviour of a single system is not studied either, but a collection of identically prepared systems, a so called *ensemble* of systems. The ensembles are isolated from the external world to some degree and there are different types of ensembles that differ in their interaction and coupling to the external world. An ensemble has an associated free energy that describes the physical behaviour [45]. One important ensemble is the canonical ensemble (NVT) with a constant number of particles N, volume V and temperature T. What constant temperature means is that the ensemble is coupled to a heat bath with constant temperature and that the ensemble is in thermal equilibrium with the heat bath. The associated free energy to the canonical ensemble is Helmholtz free energy

$$A = U - TS \tag{2.7}$$

where U is the internal energy and S the entropy. Another ensemble is Gibbs canonical ensemble (NPT), which is similar to the canonical ensemble but with constant pressure P instead of constant volume V, so in Gibbs canonical ensemble the volume can change. The Gibbs free energy is given by

$$\begin{aligned} G &= H - TS \\ &= U + PV - TS \\ &= A + PV. \end{aligned} \tag{2.8}$$

The enthalpy H includes the internal energy U and a PV term. Properties of the system are derived from the free energy and the free energy determines which state of the system that is most favourable. The free energy describes macroscopically, for example, reaction kinetics, phases and phase transitions, and solubility of mixing. The reaction kinetics, i.e. the rate of a reaction, is phenomenologically determined by Arrhenius equation [10]

$$r \propto e^{-\Delta G/k_B T} \tag{2.9}$$

where ΔG is the difference in Gibbs free energy between an initial state and the transition state

$$\Delta G = \Delta H - T\Delta S. \tag{2.10}$$

Thus, both enthalpy H and entropy S are important properties to accurately describe reactions, particularly if there are competing reaction steps and pathways, which there are in NH_3-SCR [14, 15]. As the title of this thesis suggests, focus will be on determining the entropy. However, the soon to be introduced method Thermodynamic Integration determines the anharmonic free energy and requires to some extent to calculate the internal energy U and the closely related enthalpy H, thus the internal energy is briefly presented as well.

The concept of entropy was first introduced by Boltzmann in 1877 and formalized by Planck for a system described by the microcanonical ensemble (NVE), where as opposed to the previously introduced canonical ensemble (NVT) and Gibbs ensemble (NPT), there is no interaction with the environment. In the NVE ensemble, $\Omega(N, V, E)$ denotes the number of available microscopic states, the multiplicity, of a system. The entropy was formalized as the relation [48]

$$S = k_B \ln[\Omega(N, V, E)]. \tag{2.11}$$

Entropy has multiple interpretations. A common and intuitive interpretation is that entropy is a measure of disorder [45]. A strongly adsorbed molecule, with very limited translational and rotational degrees of freedom, is in a sense ordered and has a low entropy. In this situation, the harmonic approximation (HA) works as all degrees of freedom can be approximated as vibrations. In contrast, a molecule in the gas phase has high disorder since all translations and rotations are free, and often approximated with the ideal gas law. A third possibility is the species studied in this thesis that are confined, physisorbed, in a zeolite structure with some translational and rotational freedom, but not to the extent of the gas phase. Physisorption is the phenomenon when an adsorbate is interacting with the substrate via van der Waals forces, which is a weaker bond than that of chemisorption where the adsorbate form a chemical bond, covalent or ionic, with the substrate [43]. The entropies of physisorbed adsorbates are estimated to be somewhere between the HA and ideal gas [32].

The probability of a system being in state n with energy E_n is proportional to the Boltzmann factor

$$p_n \propto e^{-\beta E_n} \tag{2.12}$$

where $\beta = 1/(k_B T)$ with Boltzman's constant k_B. The probability is normalized by dividing by the corresponding partition function Z, which is the sum over all states n

$$p_n = \frac{e^{-\beta E_n}}{\sum_n e^{-\beta E_n}} = \frac{e^{-\beta E_n}}{Z} \tag{2.13}$$

The partition function for N particles in the canonical ensemble written both as a continuous sum and an integral [45], with position $\mathbf{r} = (\boldsymbol{r}_1, ..., \boldsymbol{r}_N)$ and momentum $\mathbf{p} = (\boldsymbol{p}_1, ..., \boldsymbol{p}_N)$,

$$Z(T, V, N) = \sum_n \exp(-E_n/k_B T) = \frac{1}{h^{3N}} \int \mathrm{d}\mathbf{p}\mathrm{d}\mathbf{r} \exp\left\{-\beta \mathcal{H}(\mathbf{p}, \mathbf{r})\right\} \tag{2.14}$$

where h is Planck's constant and $\mathcal{H}$ the Hamiltonian of the system. In the canonical ensemble, we have the Helmholtz free energy, which equivalently with eq. (2.7) can be written

$$A = -k_B T \ln[Z]. \tag{2.15}$$

The thermodynamic identity for A is [46]

$$dA = -SdT - pdV + \mu dN. \tag{2.16}$$

Holding the volume V and number of molecules N fixed yields,

$$S = -\left(\frac{\partial A}{\partial T}\right)_{V,N}. \tag{2.17}$$

Inserting eq. (2.15) into eq. (2.17) yields the expression for the entropy

$$S = k_B \ln[Z] + k_B T \left(\frac{\partial \ln[Z]}{\partial T}\right)_{V,N} \tag{2.18}$$

2.4.1 Gas phase entropy

The partition function Z for a gas molecule in the ideal gas approximation consists of partition functions for translation, rotation and vibration. For the studied systems, there is no electronic multiplicity, otherwise the total number of possible spin states would also be needed to be accounted for. The partition function for a gas of N indistinguishable gas phase molecules is therefore

$$Z_{\text{gas}} = \frac{1}{N!}\left(Z_{\text{trans}} Z_{\text{rot}} Z_{\text{vib}}\right)^N \tag{2.19}$$

Using Stirlings approximation $\ln[N!] \approx N\ln[N] - N$, $N \gg 1$, yields

$$\ln[Z_{\text{gas}}] = N\left(\ln[Z_{\text{trans}}] + \ln[Z_{\text{rot}}] + \ln[Z_{\text{vib}}] - \ln[N] + 1\right) \tag{2.20}$$

The translational partition function for one gas molecule is

$$Z_{\text{trans}} = V\left(\frac{\sqrt{2\pi m k_B T}}{h}\right)^3 = \frac{V}{\nu_Q} \tag{2.21}$$

where V is the volume for a molecule, which is $V = k_B T/P$ for an ideal gas [46]. The expression is rewritten with the quantum volume ν_Q to facilitate the comparison with the expression for the CPES partition function that will be introduced below. With eq. (2.21) and the expression for the entropy in eq. (2.18) the translational component of the entropy is

$$S_{\text{trans}} = k_B\left(\ln[Z_{\text{trans}}] + \frac{5}{2}\right) \tag{2.22}$$

For the latter term, $\frac{5}{2}$, a $\frac{3}{2}$ contribution comes from the derivative of $\ln T^{3/2}$ and an 1 is the +1 in eq. (2.20) that stems from Stirling's approximation. Attributing the +1 contribution from Stirling's approximation to the translational entropy is the convention used in, for example, references [10, 14, 1]. Although the origin is configurational entropy.

Rotation for a linear rigid body, with moment of inertia I and symmetry factor σ, has the partition function [10]

$$Z_{\text{rot, linear}} = \frac{1}{\sigma}\left(\frac{8\pi^2 k_B T}{h^2}\right) I \tag{2.23}$$

from which the rotational entropy can be written using eq. (2.18)

$$S_{\text{rot,linear}} = k_B \left(\ln[Z_{\text{rot}}] + 1\right). \tag{2.24}$$

Lastly, the quantum harmonic oscillator partition function, is [32]

$$Z_{\text{vib}} = \prod_i^{N_{\text{vib}}} \frac{\exp\left(-\frac{\hbar\omega_i}{2k_BT}\right)}{1-\exp\left(-\frac{\hbar\omega_i}{k_BT}\right)}. \tag{2.25}$$

Where ω_i is the angular frequency of mode i. The number of vibrational modes N_{vib} is $3N_{\text{atoms}} - 5$ for a linear molecule, where N_{atoms} are the number of atoms. Once again, inserted into eq. (2.18) the entropy is

$$S_{\text{vib}} = k_B \sum_i \left[\frac{\hbar\omega_i}{k_BT(e^{\hbar\omega_i/k_BT}-1)} + \ln\left[1-e^{-\hbar\omega_i/k_BT}\right]\right] \tag{2.26}$$

The entropy of one molecule in gas phase is found by letting $N = 1$ in eq. (2.20), and with eq. (2.24) the gas phase entropy for a linear molecule is

$$S^{\text{gas}}_{\text{linear}} = S_{\text{trans}} + S_{\text{rot,linear}} + S_{\text{vib}}. \tag{2.27}$$

Although $N \gg 1$ is assumed when arriving at eq. (2.20), here the contribution from Stirling's approximation is included in the entropy for just one molecule. However, in reality there are many molecules and statistical mechanics are based on macroscopic behavior. We study one molecule but the results are in practice implemented for a large system. As mentioned earlier, this is also how other references treat the translational entropy.

When later comparing the ideal gas partition function with the CPES method, it is convenient to write the translational and rotation partition functions together

$$Z_{\text{trans}} Z_{\text{rot, linear}} = \frac{1}{\sigma}\left(\frac{8\pi^2 k_BT}{h^2}\right) I \frac{V}{\nu_Q}. \tag{2.28}$$

2.4.2 Gas phase internal energy and enthalpy

The expression for internal energy is similar to entropy in eq. (2.18), namely [10]

$$U = k_BT^2 \left(\frac{\partial \ln[Z]}{\partial T}\right)_{V,N}. \tag{2.29}$$

Interestingly, one can note that in the calculation of free energy $A = U - TS$, U in eq. (2.29) will be canceled by the second term in eq. (2.18). Just as for entropy, U for translation, rotation and vibration of a linear gas phase molecule can be found by inserting the partition function in eqs. (2.21), (2.28) (2.25) into eq. (2.29)

$$U_{\text{trans}} = \frac{3}{2}k_BT, \tag{2.30}$$

$$U_{\text{rot.linear}} = k_BT, \tag{2.31}$$

$$U_{\text{vib}} = \sum_{i}^{N_{\text{vib}}} \frac{1}{2}\hbar\omega_i + k_B T \sum_{i}^{N_{\text{vib}}} \left[\frac{\hbar\omega_i}{k_B T(e^{\hbar\omega_i/k_B T} - 1)} \right], \tag{2.32}$$

where the first term is denoted the zero-point energy

$$U_{\text{ZPE}} = \sum_{i}^{N_{\text{vib}}} \frac{1}{2}\hbar\omega_i. \tag{2.33}$$

Further, in the ideal gas approximation $PV = k_B T$ for a single molecule in gas phase [10], giving $H = U + k_B T$ and consequently $G = A + k_B T$. The internal energy also includes the electronic energy U_{el}. The sum of U_{el} and U_{ZPE} are also known as the internal energy at 0 K [10]. Opposed to the other terms including ω_i, U_{ZPE} depends linearly on ω_i, resulting in that soft/weak modes (low frequency) contribute less to the energy than high frequency modes. All terms combined yield the internal energy

$$U_{\text{gas,linear}} = U_{\text{el}} + U_{\text{trans}} + U_{\text{rot.linear}} + U_{\text{vib}}. \tag{2.34}$$

2.4.3 Harmonic approximation

In the harmonic approximation all degrees of freedom are treated as harmonic vibrations [32], namely the number of vibrational modes $N_{\text{vib}} = 3N_{\text{atoms}}$, in other words are translations and rotations included. The entropy is written using eq. (2.26) as

$$S_{\text{HA}} = k_B \sum_{i}^{N_{\text{vib}}} \left[\frac{\hbar\omega_i}{k_B T(e^{\hbar\omega_i/k_B T} - 1)} + \ln\left[1 - e^{-\hbar\omega_i/k_B T}\right] \right] \tag{2.35}$$

and the internal energy

$$U_{\text{HA}} = U_{\text{el}} + \sum_{i}^{N_{\text{vib}}} \frac{1}{2}\hbar\omega_i + k_B T \sum_{i}^{N_{\text{vib}}} \left[\frac{\hbar\omega_i}{k_B T(e^{\hbar\omega_i/k_B T} - 1)} \right]. \tag{2.36}$$

The free energy is therefore $A_{\text{HA}} = U_{\text{HA}} - TS_{\text{HA}}$. There is also a classical counterpart of the harmonic approximation free energy that will later be introduced in eq. (2.64).

2.5 Complete Potential Energy Sampling (CPES)

The restricted translations and rotations of an adsorbed linear molecule are described by the partition function [32]

$$Z^{\text{CPES}}_{\text{trans,rot,linear}} = \frac{1}{\sigma}\left(\frac{8\pi^2 k_B T}{h^2}\right) I \frac{1}{\nu_Q} \int_{u.c.} e^{-U(\mathbf{r},\mathbf{\Phi})/k_B T} \mathrm{d}\mathbf{r}\mathrm{d}\mathbf{\Phi} \tag{2.37}$$

where $\mathbf{r}$ is the position of the center of mass of the adsorbed molecule, $\mathbf{\Phi}$ the generalized rotational angles (Euler angles) $\mathbf{\Phi} = (\theta/\pi, \phi/2\pi, \psi/2\pi)$ describing rotations of a rigid body, which the molecule is assumed to be. The integration is over the unit cell (u.c.). The potential energy $U(\mathbf{r}, \mathbf{\Phi})$ is the relative potential energy surface (PES) of translations and rotations of the adsorbed molecule, i.e.

$$U(\mathbf{r}, \mathbf{\Phi}) = E_{\mathrm{A@S}} - E_{\mathrm{S}} - E_{\mathrm{A}} \tag{2.38}$$

where S is the substrate in which the adsorbate A is adsorbed, and the combined system is A@S, and E denotes the energy of respective system. Note that the vibrations are not included in $U(\mathbf{r}, \mathbf{\Phi})$.

The difference between the partition function for translation and rotation in the ideal gas in eq. (2.28) and for CPES in eq. (2.37) is that the volume V has been replaced by the integral $\int_{u.c.} e^{-U(\mathbf{r},\mathbf{\Phi})/k_BT} \mathrm{d}\mathbf{r}\mathrm{d}\mathbf{\Phi}$. As the angles describing rotations ($\mathbf{\Phi}$) are unitless, the unit of the integral is volume (m^3). The integral can be interpreted as the volume in which the adsorbed molecule is allowed to translate and rotate. If, for example, the molecule is close to a steep potential energy wall, the hindered rotation is captured by the integral. As the partition function otherwise is exactly the same as for translation and rotation of an ideal gas, the integral can also be seen as a scaling factor of how many configurations, or entropy, are lost at adsorption in the confined zeolite. One can also observe that the lowest energy $U(\mathbf{r}, \mathbf{\Phi})$ configurations give the largest contributions to eq. 2.37.

Further interpretation of the integral is required since the volume is fixed in the derivative in eq. (2.17). This might pose a problem if the value of the integral is seen as the volume. First, we consider the important property of $Z^{\mathrm{CPES}}_{\mathrm{trans,rot,linear}}$ that the entropy is invariant to an arbitrary shift in the potential $U(\mathbf{r}, \mathbf{\Phi})$. Let us imagine a free gas molecule, whether the reference energy of the flat potential energy surface is 0 or 100 eV should not affect the entropy, since the molecule experiences a flat surface. This is shown by considering a shift U_0 for the energy in the exponent in the integral in eq. (2.37) and using eq. (2.15) and (2.17). Since the entropy is dependent on the logarithm of the partition function, it is enough to consider only the integral of the CPES partition function in eq. (2.37) to show the invariance

$$\begin{aligned}
S = &- \frac{\partial}{\partial T}\left(-k_BT \ln\left[\int_{u.c.} e^{-(U(\mathbf{r},\mathbf{\Phi})+U_0)/k_BT}\mathrm{d}\mathbf{r}\mathrm{d}\mathbf{\Phi}\right]\right)_{V,N} = \\
&- \frac{\partial}{\partial T}\left(-k_BT \ln\left[e^{-U_0/k_BT}\int_{u.c.} e^{-U(\mathbf{r},\mathbf{\Phi})/k_BT}\mathrm{d}\mathbf{r}\mathrm{d}\mathbf{\Phi}\right]\right)_{V,N} = \\
&- \frac{\partial}{\partial T}\left(-k_BT \left(\frac{-U_0}{k_BT}\right) - k_BT \ln\left[\int_{u.c.} e^{-U(\mathbf{r},\mathbf{\Phi})/k_BT}\mathrm{d}\mathbf{r}\mathrm{d}\mathbf{\Phi}\right]\right)_{V,N} = \\
&- \frac{\partial}{\partial T}\left(-k_BT \ln\left[\int_{u.c.} e^{-U(\mathbf{r},\mathbf{\Phi})/k_BT}\mathrm{d}\mathbf{r}\mathrm{d}\mathbf{\Phi}\right]\right)_{V,N}.
\end{aligned} \tag{2.39}$$

Thus, the entropy does not depend on the shift U_0. To investigate the effect of the volume, we will see that the shown invariance leads to that the fixed volume in the derivative in the entropy can be omitted for the integral. Consider the second term in the expression for the entropy in eq. (2.18).

$$k_BT\left(\frac{\partial \ln[Z]}{\partial T}\right)_{V,N} \tag{2.40}$$

and again only use the integral in eq. (2.37) with an energy shift U_0 for the partition function, yielding

$$\begin{aligned} &k_B T \frac{\partial}{\partial T} \ln \left[\int_{u.c.} e^{-(U(\mathbf{r},\mathbf{\Phi})+U_0)/k_B T} \mathrm{d}\mathbf{r}\mathrm{d}\mathbf{\Phi} \right] = \\ &k_B T \frac{\partial}{\partial T} \left(-\frac{U_0}{k_B T} + \ln \left[\int_{u.c.} e^{-U(\mathbf{r},\mathbf{\Phi})/k_B T} \mathrm{d}\mathbf{r}\mathrm{d}\mathbf{\Phi} \right] \right) = \\ &\frac{U_0}{T} + \frac{\int_{u.c.} \frac{U(\mathbf{r},\mathbf{\Phi})}{T} e^{-U(\mathbf{r},\mathbf{\Phi})/k_B T} \mathrm{d}\mathbf{r}\mathrm{d}\mathbf{\Phi}}{\int_{u.c.} e^{-U(\mathbf{r},\mathbf{\Phi})/k_B T} \mathrm{d}\mathbf{r}\mathrm{d}\mathbf{\Phi}} \end{aligned} \tag{2.41}$$

This is equal to the ensemble average $\langle (U(\mathbf{r},\mathbf{\Phi}) + U_0 \rangle / T$, which obviously can be zero if an appropriate U_0 is chosen. The expression in eq. (2.41) is zero if we let the shift be

$$U_0 = -\frac{\int_{u.c.} U(\mathbf{r},\mathbf{\Phi}) e^{-U(\mathbf{r},\mathbf{\Phi})/k_B T} \mathrm{d}\mathbf{r}\mathrm{d}\mathbf{\Phi}}{\int_{u.c.} e^{-U(\mathbf{r},\mathbf{\Phi})/k_B T} \mathrm{d}\mathbf{r}\mathrm{d}\mathbf{\Phi}} \tag{2.42}$$

So, with the shift U_0, we have that the contribution from the integral to the entropy from the latter term in eq. (2.18) is zero, i.e.

$$\left(\frac{\partial \ln \left[\int_{u.c.} e^{-(U(\boldsymbol{r},\mathbf{\Phi})+U_0)/k_B T} \mathrm{d}\mathbf{r}\mathrm{d}\mathbf{\Phi} \right]}{\partial T} \right)_{V,N} = 0 \tag{2.43}$$

which means that the volume, i.e. the integral, can also be kept fixed for $Z^{\mathrm{CPES}}_{\mathrm{trans,rot,linear}}$ without omitting any contributions. In practice, however, the explicit value of U_0 is not required since the entropy is independent of the choice of shift, as shown in eq. (2.39).

Vibrations are treated with the harmonic approximation, i.e. the vibrational entropy is the same as for an ideal gas, calculated with eq. (2.26). With eqs. (2.18) and (2.37), we have the final adsorbate entropy with the CPES method

$$S^{\mathrm{CPES}}_{\mathrm{linear}} = S_{\mathrm{vib}} + k_B \left(\ln Z^{\mathrm{CPES}}_{\mathrm{trans,rot,linear}} + \frac{7}{2} + \frac{\int_{u.c.} \frac{U(\mathbf{r},\mathbf{\Phi})}{k_B T} e^{-U(\mathbf{r},\mathbf{\Phi})/k_B T} \mathrm{d}\mathbf{r}\mathrm{d}\mathbf{\Phi}}{\int_{u.c.} e^{-U(\mathbf{r},\mathbf{\Phi})/k_B T} \mathrm{d}\mathbf{r}\mathrm{d}\mathbf{\Phi}} \right). \tag{2.44}$$

Furthermore, the entropy contribution from only CPES, i.e. translations and rotations, can be defined for a linear molecule as

$$S^{\mathrm{CPES}}_{\mathrm{trans,rot,linear}} = S^{\mathrm{CPES}}_{\mathrm{linear}} - S_{\mathrm{vib}}. \tag{2.45}$$

The entropy with CPES can also be described as a fraction of the gas phase entropy as

$$S^{\mathrm{CPES}}_{\mathrm{linear}} = S_{\mathrm{vib}} + \gamma (S^{\mathrm{gas}}_{\mathrm{trans}} + S^{\mathrm{gas}}_{\mathrm{rot,linear}}). \tag{2.46}$$

Note that γ is a measure of how restricted the translations and rotations are.

2.6 Thermodynamic integration (TI)

Within the canonical ensemble, it is the Helmholtz free energy difference that is of interest. Thermodynamic integration (TI) is a method to compute the free energy difference between two systems [48, 20], and two general systems will here be denoted system $\mathcal{A}$ and $\mathcal{B}$. Here is first the fundamentals of thermodynamic integration presented. Secondly, the TI scheme in [1] implemented in this report is presented, where TI is extended with a transformation to internal coordinates.

2.6.1 Fundamentals

Before introducing TI, a straightforward method to write the Helmholtz free energy difference between systems $\mathcal{A}$ and $\mathcal{B}$ is

$$\Delta A_{\mathcal{A}\longrightarrow\mathcal{B}} = A_{\mathcal{B}} - A_{\mathcal{A}} \tag{2.47}$$

and with $A = -k_B T \ln Z$

$$\Delta A_{\mathcal{A}\longrightarrow\mathcal{B}} = -k_B T \ln \frac{Z_{\mathcal{B}}}{Z_{\mathcal{A}}}. \tag{2.48}$$

Here, $Z_{\mathcal{A}}$ and $Z_{\mathcal{B}}$ are the partition functions

$$Z_{\mathcal{A}(\mathcal{B})} = \int \mathrm{d}\mathbf{r} e^{-U_{\mathcal{A}(\mathcal{B})}(\mathbf{r})/k_B T} \tag{2.49}$$

as the momentum contribution is cancelled in the ratio in (2.48) [48]. Access to the partition functions is required to use (2.48), which for more complex systems is difficult. It is possible to rewrite the equation using perturbation theory to get $\Delta A_{\mathcal{A}\longrightarrow\mathcal{B}} = -k_B T \ln \left\langle e^{-(U_{\mathcal{B}}-U_{\mathcal{A}})/k_B T} \right\rangle_{\mathcal{A}}$, but the convergence of this average is slow when the overlap between the systems $\mathcal{A}$ and $\mathcal{B}$ is small [48]. An approach to circumvent a direct switch between the systems is thermodynamic integration, where the initial system ($\mathcal{A}$) continuously merges into the final system ($\mathcal{B}$).

The Hamiltonian that describe the intermediate systems between $\mathcal{A}$ and $\mathcal{B}$ is with the coupling parameter λ defined as

$$\mathcal{H}_\lambda = \lambda \mathcal{H}_{\mathcal{B}} + (1-\lambda)\mathcal{H}_{\mathcal{A}}, \tag{2.50}$$

with the intermediate potential energy

$$U_\lambda = \lambda U_{\mathcal{B}} + (1-\lambda) U_{\mathcal{A}} \tag{2.51}$$

and the kinetic energy $\hat{K}$, the intermediate Hamiltonian can be written as

$$\mathcal{H}_\lambda = \hat{K} + U_\lambda. \tag{2.52}$$

Note that for $\lambda = 0$, the initial system is recovered and for $\lambda = 1$, the final system is recovered. By gradually increasing λ, the system slowly switch from $\mathcal{A}$ to $\mathcal{B}$ [48]. The canonical partition function Q_λ, which includes the partition function Z_λ from eq. (2.49), is

$$Q_\lambda = \frac{1}{N!h^{3N}} \int \mathrm{d}\mathbf{p}\mathrm{d}\mathbf{r} \exp\left\{-\beta\left[\sum_{i=1}^{N} \frac{\boldsymbol{p}_i^2}{2m_i} + U_\lambda(\boldsymbol{r}_1, ..., \boldsymbol{r}_N)\right]\right\} \tag{2.53}$$

As earlier in section 2.4, we have position $\mathbf{r} = (\boldsymbol{r}_1, ..., \boldsymbol{r}_N)$ and momentum $\mathbf{p} = (\boldsymbol{p}_1, ..., \boldsymbol{p}_N)$. With this partition function, the Helmholtz free energy is $A_\lambda = -k_B T \ln Q_\lambda$.

Next, we note that the Helmholtz free energy difference can be obtained from

$$\Delta A_{\mathcal{A}\longrightarrow\mathcal{B}} = A(\lambda = 1) - A(\lambda = 0) = \int_0^1 \frac{\partial A(\lambda)}{\partial \lambda} \mathrm{d}\lambda. \tag{2.54}$$

The derivative $\partial A_\lambda / \partial \lambda$ can be written

$$\frac{\partial A_\lambda}{\partial \lambda} = \frac{-k_B T}{Q_\lambda} \frac{\partial Q_\lambda}{\partial \lambda} = \frac{-k_B T}{Z_\lambda} \frac{\partial Z_\lambda}{\partial \lambda}. \tag{2.55}$$

As before, the kinetic energy $\hat{K}$ (or momentum contribution) is canceled, we are only left with the configurational partition function Z_λ in (2.49), yielding

$$\begin{aligned} \frac{-k_B T}{Z_\lambda} \frac{\partial Z_\lambda}{\partial \lambda} &= \frac{k_B T}{Z_\lambda} \frac{\partial}{\partial \lambda} \int \mathrm{d}\mathbf{r} e^{-U_\lambda(\boldsymbol{r}_1, ..., \boldsymbol{r}_N)/k_B T} \\ &= \frac{k_B T}{Z_\lambda} \int \mathrm{d}\mathbf{r} \left(-\frac{1}{k_B T} \frac{\partial U_\lambda}{\partial \lambda}\right) \exp\left\{-U_\lambda(\boldsymbol{r}_1, ..., \boldsymbol{r}_N)/k_B T\right\} \\ &= \left\langle \frac{\partial U_\lambda}{\partial \lambda} \right\rangle_\lambda \end{aligned} \tag{2.56}$$

Using eq. (2.51), we see that

$$\frac{\partial U_\lambda}{\partial \lambda} = U_\mathcal{B} - U_\mathcal{A} \tag{2.57}$$

The result from eqs. (2.55), (2.56) and (2.57) can be summarized

$$\frac{\partial A_\lambda}{\partial \lambda} = \langle U_\mathcal{B} - U_\mathcal{A} \rangle_\lambda . \tag{2.58}$$

With this expression, eq. (2.58), inserted into eq. (2.54) we have

$$\Delta A_{\mathcal{A}\longrightarrow\mathcal{B}} = \int_0^1 \left\langle \frac{\partial U_\lambda}{\partial \lambda} \right\rangle_\lambda \mathrm{d}\lambda = \int_0^1 \langle U_\mathcal{B} - U_\mathcal{A} \rangle_\lambda \, \mathrm{d}\lambda. \tag{2.59}$$

Using equation (2.59), the free energy difference is found by calculating the ensemble average of the energy difference $U_\mathcal{B} - U_\mathcal{A}$ for a system driven by the potential U_λ for a number of λ-values. By definition of the ensemble average, we can write the analytic expression for the ensemble average as [48]

$$\langle U_\mathcal{B} - U_\mathcal{A} \rangle_\lambda = \frac{\int \mathrm{d}\boldsymbol{r} \left[U_\mathcal{B} - U_\mathcal{A}\right] \exp\left(-U_\lambda(\boldsymbol{r})/k_B T\right)}{\int \mathrm{d}\boldsymbol{r} \exp\left(-U_\lambda(\boldsymbol{r})/k_B T\right)}. \tag{2.60}$$

Since the ensemble average is to be sampled in this method, we need to shortly discuss what is required from the molecular dynamics. From MD we can compute

the time average. If we assume that the system is ergodic and that the selected thermostat described the ensemble correctly, the time average will be equivalent to the ensemble average [45].

2.6.2 TI with a harmonic reference system

Thermodynamic integration is in ref. [1] implemented with a harmonic reference system as the initial system and the fully interacting DFT-based system as the final system to compute the adsorption free energy. The harmonic reference system is vibrations, rotations and translations described by harmonic potentials, i.e. the harmonic approximation. By using thermodynamic integration, the anharmonic contributions to the harmonic approximation can be calculated by switching to the final system driven by DFT. The method is further extended to using internal coordinates, denoted $\boldsymbol{q}$, that aim to speed up convergence [1], which is presented in more detail below in section 2.6.3.

To emphasize the specific implementation, compared to the more general theory on TI in the previous section, and to be consistent with the TI reference [1], new notation for the initial och final system is introduced. The harmonic reference system in cartesian coordinates is denoted $0, \boldsymbol{x}$, the harmonic reference system in internal coordinates is denoted $0, \boldsymbol{q}$ and the true physical system computed with DFT is denoted 1. Re-arranging the terms in eq. (2.54) yields the Helmholtz free energy of system 1

$$A_1 = A_{0,\boldsymbol{x}} + \Delta A_{0,\boldsymbol{x}\longrightarrow 0,\boldsymbol{q}} + \Delta A_{0,\boldsymbol{q}\longrightarrow 1} \tag{2.61}$$

where $A_{0,\boldsymbol{x}}$ is the free energy of the harmonic system in cartesian coordinates $\boldsymbol{x}$, $\Delta A_{0,\boldsymbol{x}\longrightarrow 0,\boldsymbol{q}}$ is the free energy contribution by the transformation from the system harmonic in $\boldsymbol{x}$ to harmonic in internal coordinates $\boldsymbol{q}$. The last term $\Delta A_{0,\boldsymbol{q}\longrightarrow 1}$ is the contribution when finally switching from the harmonic system in $\boldsymbol{q}$ to the fully interacting system 1 that is described by DFT. Both terms $\Delta A_{0,\boldsymbol{x}\longrightarrow 0,\boldsymbol{q}}$ and $\Delta A_{0,\boldsymbol{q}\longrightarrow 1}$ is calculated using eq. (2.59).

The harmonic approximation in $\boldsymbol{x}$ gives the harmonic potential

$$V_{0,\boldsymbol{x}}(\boldsymbol{x}) = V_{0,\boldsymbol{x}}(\boldsymbol{x}_0) + \frac{1}{2}(\boldsymbol{x}-\boldsymbol{x}_0)^T \boldsymbol{H}^{\boldsymbol{x}}(\boldsymbol{x}-\boldsymbol{x}_0) \tag{2.62}$$

$\boldsymbol{x}_0$ corresponds to the ground state structure and $\boldsymbol{H}^{\boldsymbol{x}}{}_{i,j} = \frac{\partial^2 V_{0,\boldsymbol{x}}(\boldsymbol{x})}{\partial \boldsymbol{x}_i \boldsymbol{x}_j}|_{\boldsymbol{x}=\boldsymbol{x}_0}$. The harmonic free energy in $\boldsymbol{x}$ writes

$$A_{0,\boldsymbol{x}} = A_{\mathrm{el}}(\boldsymbol{x}_0) + A_{\mathrm{vib}} \tag{2.63}$$

where $A_{\mathrm{el}}(\boldsymbol{x}_0)$ is the electronic free energy and if the multiplicity of the ground state is 1 then $A_{\mathrm{el}}(\boldsymbol{x}_0) = V_0(\boldsymbol{x}_0)$, which is the case for our studied systems. The second term A_{vib}, contains all degrees of freedom and is here treated as vibrations within the classical harmonic approximation, as the difference in adsorption free energy compared to its quantum counterpart is negligible at the studied temperatures (above

200 K) [1]. With number of modes N_{vib} and angular frequency ω_i of mode i, the classical vibrational free energy is [48, 45] in the classical limit $k_BT \gg \hbar\omega$

$$A_{\text{vib}} = -k_BT \sum_{i=1}^{N_{\text{vib}}} \ln \frac{k_BT}{\hbar\omega}. \tag{2.64}$$

The second term in eq. (2.61), $\Delta A_{0,\boldsymbol{x}\longrightarrow 0,\boldsymbol{q}}$, is the correction term belonging to the coordinate transformation from cartesian $\boldsymbol{x}$ to the internal coordinates $\boldsymbol{q}$. The momentum part $\hat{K}$ of the Hamiltonian driving the system is independent of coordinate system [1], so we have the Hamiltonian $\mathcal{H}_\lambda = \lambda\mathcal{H}_{0,\boldsymbol{q}} + (1-\lambda)\mathcal{H}_{0,\boldsymbol{x}} = \hat{K} + V_\lambda$ for a $\lambda \in [0,1]$ with the intermediate potential energy

$$V_\lambda = \lambda V_{0,\boldsymbol{q}} + (1-\lambda)V_{0,\boldsymbol{x}}. \tag{2.65}$$

Using eq. (2.59), the correction is found as

$$\Delta A_{0,\boldsymbol{x}\longrightarrow 0,\boldsymbol{q}} = \int_0^1 \langle V_{0,\boldsymbol{q}} - V_{0,\boldsymbol{x}} \rangle_\lambda \, \mathrm{d}\lambda \tag{2.66}$$

Similarly for the third term in eq. (2.61), $\Delta A_{0,\boldsymbol{q}\longrightarrow 1}$, but now the MD is driven by the Hamiltonian $\mathcal{H}_\lambda = \lambda\mathcal{H}_1 + (1-\lambda)\mathcal{H}_{0,\boldsymbol{q}}$ to switch the system from harmonic internal coordinates $0, \boldsymbol{q}$ to the fully interacting, DFT driven, system 1. The corresponding correction term is

$$\Delta A_{0,\boldsymbol{q}\longrightarrow 1} = \int_0^1 \langle V_1 - V_{0,\boldsymbol{q}} \rangle_\lambda \, \mathrm{d}\lambda. \tag{2.67}$$

2.6.3 Internal coordinates

For systems as gas-phase molecules and weakly adsorbed molecules, direct use of cartesian coordinates is not practical due to their energy insensitivity to overall rotations and translations outside the region of their minima. This might lead to difficulties reaching convergence of the average $\langle V_1 - V_{0,\boldsymbol{x}} \rangle_\lambda$ and required many expensive DFT calculations. To circumvent this problem, translationally and rotationally invariant internal coordinates $\boldsymbol{q}$ are implemented as an intermediate step in the TI procedure to account for the translations and rotations of these systems. Sampling $\langle V_{0,\boldsymbol{q}} - V_{0,\boldsymbol{x}} \rangle_\lambda$ is considerably computationally cheaper than involving V_1 (DFT).

The internal coordinates are bond lengths (interatomic distances), angles, torsions and coordination numbers (CN). The extra correction term $\Delta A_{0,\boldsymbol{x}\longrightarrow 0,\boldsymbol{q}}$ is required since the forcefield that is harmonic in the cartesian coordinates $\boldsymbol{x}$ can be different than the harmonic forcefield in internal coordinates $\boldsymbol{q}$. Rules for choosing internal coordinates are presented for the different subsystems:

- Molecules and special flexible sites, such as Brønstedt sites: bond lengths, bond angles and torsion angles.
- Substrate: For all atoms in the substrate, interatomic distances with atoms from the first three coordination spheres.

- Adsorbed molecule: the position and rotation of the molecule are described by coordination numbers (CNs) to atoms in the substrate.

For an atom i of the molecule with respect to an atom j in the substrate is the CN defined as

$$\mathrm{CN}_i = \sum_{j}^{N_{\mathrm{sub}}} \sum_{\boldsymbol{L}} \frac{1 - (r_{ij,\boldsymbol{L}}/R_{ij})^9}{1 - (r_{ij,\boldsymbol{L}}/R_{ij})^{14}} \tag{2.68}$$

with all or selected substrate atoms N_{sub} in a unit cell. The sum is also over translations, $\boldsymbol{L} = \{\pm l_1, l_2, l_3\}$, of the unit cell with lattice vectors $\boldsymbol{a}_i$. So the distance $r_{ij,\boldsymbol{L}}$ is between molecule atom i and substrate atom j translated by $l_1\boldsymbol{a}_1 + l_2\boldsymbol{a}_2 + l_2\boldsymbol{a}_2$ from the original unit cell $\boldsymbol{L} = \{0, 0, 0\}$. $\boldsymbol{L}$ is truncated when $r_{ij,\boldsymbol{L}}$ exceeds 30 Å. Lastly, R_{ij} is the reference distance between atom i and atom j. The CN is a smooth function that is describing with a number between 0 and 1 depending on how close atoms i and j are. Atoms that are close have CN near 1 and atoms far away have a CN that is 0. Further rules are to exclude angles in the relaxed structure that are above 165°, to avoid numerical problems with straight angles (180°) [1].

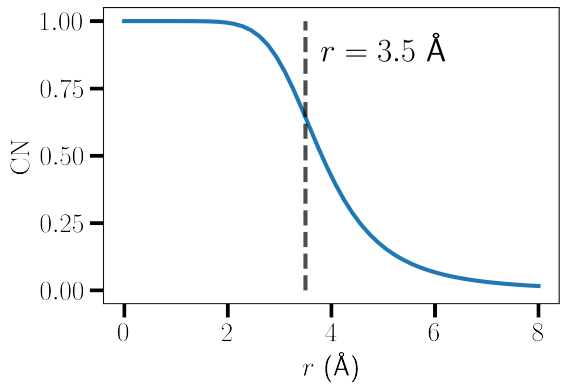

Figure 2.1: Coordination number CN plotted against r with reference distance $R = 3.5$ Å. Note, the CN in the figure is a single term in the sum in eq. (2.68).

2.6.4 Special case: diatomic bond length

For the special case of having a diatomic molecule, the interatomic distance is the internal coordinate, hence an explicit semi-analytical solution of the correction term(s) can be derived, see eqs. (2.69) and (2.70). The (harmonic) forcefield-forcefield transformation term $\Delta A_{0,\boldsymbol{x}\longrightarrow 0,\boldsymbol{q}}$ is zero due to that an interatomic distance is phase space conserving and a quasi one dimensional coordinate, which corresponds to the $\boldsymbol{q}$ coordinate [1]. From earlier results in the fundamentals section, we can write the reference free energy A^{ref} with eq. (2.48) as in [1] using spherical coordinates and noting the rotational invariance

$$\Delta A^{\mathrm{ref}}_{0,\boldsymbol{q}\longrightarrow 1} = -\frac{1}{\beta} \ln \left[\frac{\int_{R_{\mathrm{min}}}^{R_{\mathrm{max}}} \mathrm{d}R R^2 \exp\left\{-\beta V_1(R)\right\}}{\int_{R_{\mathrm{min}}}^{R_{\mathrm{max}}} \mathrm{d}R R^2 \exp\left\{-\beta V_{0,\boldsymbol{q}}(R)\right\}} \right]. \tag{2.69}$$

Using the expression in eq. (2.60) for the average in eq. (2.67) we can write

$$\langle V_1 - V_{0,\boldsymbol{q}} \rangle_\lambda^{\text{ref}} = \frac{\int_{R_{\min}}^{R_{\max}} \mathrm{d}R R^2 (V_1(R) - V_{0,\boldsymbol{q}}(R)) \exp\{-\beta V_\lambda(R)\}}{\int_{R_{\min}}^{R_{\max}} \mathrm{d}R R^2 \exp\{-\beta V_\lambda(R)\}} \tag{2.70}$$

The notation "ref" indicates the exact semi-analytical reference value.

2.6.5 Entropy from TI

A problem emerging due to the scope of this thesis is that the TI method results in an anharmonic free energy, while we are interested in the entropy. Obviously, this does not pose a problem if the end goal is to find accurate free energies which usually is the case. However, to compare the results from TI with CPES, the entropy has to be extracted from the free energy. To do this, firstly the previous assumption to use the high temperature approximation (classical) vibrational free energy is exchanged to the non-approximated (quantum) counterpart presented in section 2.4.3, which is required to separate the entropy and internal energy individually from the free energy.

It is assumed that harmonic approximation with the unmodified eigenvalues approximates U_{ZPE} well. In other words, the increase in the zero-point energy due to the increased eigenvalues, where low frequency modes stemming from translations and rotations gets increased frequency, are compensated fully by the anharmonic correction terms.

Denote the combined correction term

$$\Delta A_{\text{corr.}} = \Delta A_{0,\boldsymbol{x}\longrightarrow 0,\boldsymbol{q}} + \Delta A_{0,\boldsymbol{q}\longrightarrow 1}. \tag{2.71}$$

And the ZPE compensated correction term

$$\Delta A'_{\text{corr.}} = \Delta A_{\text{corr.}} + \Delta U_{\text{ZPE}} \tag{2.72}$$

where the difference in zero-point energy is defined as

$$\Delta U_{\text{ZPE}} = U_{\text{ZPE,mod.}} - U_{\text{ZPE,unmod.}}. \tag{2.73}$$

From HA internal energy and entropy in eqs. (2.36) and (2.35) and noting the TS_{HA} and U_{HA} share a term, we define

$$\alpha_{\text{S}} = \frac{\sum_i^{N_{\text{vib}}} \left[\frac{\hbar\omega_i}{k_B T (e^{\hbar\omega_i / k_B T} - 1)} + \ln\left[1 - e^{-\hbar\omega_i / k_B T}\right] \right]}{\sum_i^{N_{\text{vib}}} \left[2 \cdot \frac{\hbar\omega_i}{k_B T (e^{\hbar\omega_i / k_B T} - 1)} + \ln\left[1 - e^{-\hbar\omega_i / k_B T}\right] \right]} \tag{2.74}$$

that represents the fraction of the anharmonic correction that will be attributed to the entropy as

$$TS_1 = TS_0 - \Delta A'_{\text{corr.}}\alpha_{\text{S}}. \tag{2.75}$$

Where, to reiterate, S_1 is the anharmonic entropy from TI and S_0 is the entropy from the harmonic approximation with the modified eigenvalues. In other words, the fraction of the anharmonic correction is directly proportional to the size of the vibrational contribution to the entropy compared to the internal energy. But once again, the problem of requiring extraction of the entropy from the free energy gained from the TI method is primarily due to the scope of the thesis.

3
Methods

In this chapter, the studied molecular structures are shown. The software, methods and parameters for the calculations are also presented, and lastly, the CPES and TI methods are presented. Data analysis was done in Python with the packages Numpy [24] and Scipy [49], via which the Qhull [4] algorithm was used for interpolation. For plotting, matplotlib [28] and corner [17] were used. The atom structures were handled with ASE [40].

3.1 Molecular structures

In this thesis, the terminology adsorbate and substrate will extensively be used. Adsorbate means the molecule, here N_2 and $[Cu(NH_3)_2]^+$, that is adsorbed inside the zeolite, where the zeolite is the substrate. The studied zeolites were the chabazite silicalite, denoted CHA$-SiO_2$, of which a unit cell consists of 24 O and 12 Si atoms. The SSZ-13 with a 1/11 Al/Si ratio with H^+ as counter ion, denoted H-CHA, and lastly the same structure as H-CHA but with the H^+ removed, denoted CHA. A rhombohedral unit cell was used for the chabazite structure with the experimentally determined lattice parameters ($\alpha = \beta = \gamma = 94.2°, a = b = c = 9.42$ Å) [14, 15]. During atomic structure relaxations, the lattice parameters were held fixed. Mass of tritium (3u) has consistently been used for hydrogen through the work to allow for a larger timestep, a substitution used in other references [1, 14].

The studied adsorption cases were N_2 adsorbed in H-CHA and CHA$-SiO_2$, and $[Cu(NH_3)_2]^+$ adsorbed CHA. The structures are seen in fig. 3.1a, 3.1b and 3.1c, respectively. The atom color code is: oxygen O (red), silicon Si (beige), nitrogen N (blue), aluminum Al (grey), hydrogen H (white) and copper Cu (brown). Additionally, a simple gas phase molecule, hydrogen fluoride HF was studied in the TI method.

3.2 DFT and MD

The Vienna Ab initio Simulation Package (VASP) [35, 36, 37] was used for all density functional theory (DFT) calculations, including relaxation, vibrational analysis and molecular dynamics (MD). VASP was therefore used in all CPES calculations and simulations. The Thermodynamic Integration (TI) method is implemented in VASP, meaning that the correction term $\Delta A_{0,q\longrightarrow 1}$ was calculated using VASPs

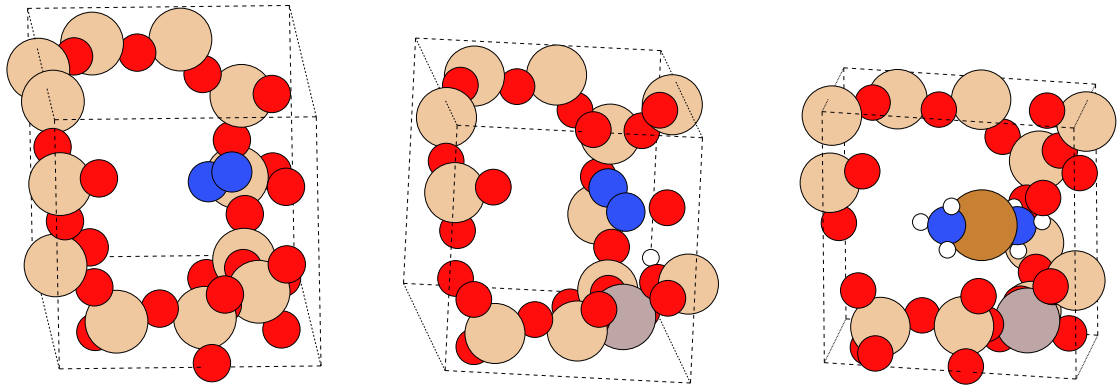

(a) **(b)** **(c)**

Figure 3.1: Studied adsorption structures. (a): N_2 adsorbed in CHA−SiO_2. (b): N_2 adsorbed in H-CHA. (c): $[Cu(NH_3)_2]^+$ adsorbed in CHA. Atom colors are oxygen O (red), silicon Si (beige), nitrogen N (blue), aluminum Al (grey), hydrogen H (white) and copper Cu (brown).

MD. However, for the other correction term, the forcefield-forcefield transformation $\Delta A_{0\boldsymbol{x}\longrightarrow 0,\boldsymbol{q}}$, was a harmonic molecular dynamics (hMD) program used. The hMD program was provided by Bučko [1], who also provided other programs to generate the Hessian matrix from the vibrational analysis from VASP, as well as other utilities to setup the internal coordinates and calculate different free energy contributions and averages.

In VASP, a plane wave basis set describes the valence electrons. A convergence test of the plane wave basis cut-off energy was performed and showed convergence at 480 eV, which is consistent with other relevant references [14, 15]. However, when N_2 in H-CHA is reproduced, a cut-off of 400 eV [1] was used. The valence electron-core electron interactions are described with the projector augmented wave (PAW) method [6, 38]. The sampling of the Brillouin zone was restricted to the gamma point.

As mentioned in the DFT theory in section 2.2, the exchange correlation is important and difficult to describe. In this thesis the PBE [44] functional is used, augmented with two different approaches to account for the van der Waals interactions, namely D2 [22] and D3 [23]. Accurate van der Waals forces are important due to the physisorbed nature of the studied adsorption problems. Structures including the $[Cu(NH_3)_2]^+$ complex has also a, so called, Hubbard [3] term added, where the U parameters were set to 6 eV for Cu 3d [14], to describe highly localized Cu 3d electrons [14]. For all CPES calculations and the HF molecule in TI was 10^{-6} eV used as convergence criteria for the SCF loop, while 10^{-7} eV was used in the other TI simulations. Once again, this was to be able to reproduce the results of the TI reference [1] as close as possible. The conjugate gradient algorithm implemented in VASP was used for the structure relaxations and the convergence criteria used for the forces on each atom was 0.005 eV/Å.

The vibrational analysis to find the eigenmodes, and mainly, the eigenvalues were done in VASP using central finite differences, where a displacement of 0.015 Å of each atom in positive and negative cartesian coordinate direction, i.e. 6 displacements per atom, to calculate the second derivatives of the Hessian matrix.

Other method specific parameters are presented in its corresponding method section, as for example thermostat for MD and van der Waals correction. For molecules in gas phase, the same unit cell size as for the zeolites was used. All simulations were computed using Chalmers's C3SE computational resources.

3.3 CPES

For all CPES MD simulations the Nosé-Hoover thermostat was used to keep a temperature of 473 K. A time step of 1 fs was used for all MD and MTD simulations, except with regular MD for N_2@H-CHA between 10 and 25 ps in the production run, see fig. 4.6. In this time interval, a short time step of 0.5 fs was used to do a short investigation of any change in dynamics, but no difference could be seen, which should be the case. Therefore, the trajectory data was deemed appropriate to reuse in the sampling of the PES.

3.3.1 Framework

Earlier studies of adsorption entropy using CPES, with both a Monte Carlo (MC) scheme [32] and metadynamics [12], have used a fixed zeolite framework, meaning that all the atoms of the zeolite are fixed during MC or MD, while the adsorbate is unconstrained in the zeolite. However, other studies show that the fixed zeolite framework influences diffusion and adsorption energy. Having a flexible, dynamic, zeolite framework is of importance and should not be neglected [41, 8]. A comparison of the distance traveled by the center of mass of a N_2 molecule in H-CHA was done with two MD simulations with the dynamic and fixed framework at 473 K, seen in fig. 4.4.

The reasoning behind the fixed framework for MD was to eliminate the vibrations of the zeolite from the total energy, although the vibrations from the adsorbate are still present and need to be eliminated, which has been solved in other works with a rolling average and a low pass filter [12]. However, this post-processing was simple for small molecules as N_2 but showed to be tedious to perform on the simulation data for large adsorbates with many vibrational modes as for example $[Cu(NH_3)_2]^+$.

To include the dynamic framework and circumvent the post-processing with filters, an adapted approach to earlier implementations of CPES was implemented. After an MD simulation with dynamic framework, the adsorbate was removed from the zeolite and the instantaneous energy of the molecule (N_2 or $[Cu(NH_3)_2]^+$) and the clean zeolite substrate (CHA$-SiO_2$, H-CHA or CHA) was re-calculated, with

the exact same atomic configuration as in the MD simulation. This procedure is demonstrated in fig. 3.2. Every 4th step, i.e. every 4 fs, was recalculated. This step size was concluded to be sufficient, see fig. 4.3 in section 4.1.1. With the energies of the three systems, $E_{\text{A@S}}, E_{\text{S}}$ and E_{A}, was the relative potential energy surface in eq. (2.38) calculated.

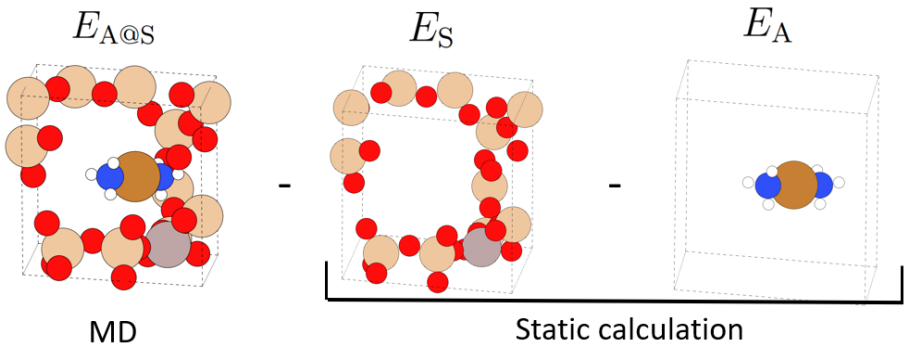

Figure 3.2: Illustration how eq. (2.38) $U(\mathbf{r}, \mathbf{\Phi}) = E_{\text{A@S}} - E_{\text{S}} - E_{\text{A}}$ is calculated in this thesis. MD of the full dynamic system is first simulated, then the adsorbate is lifted out of the zeolite substrate and for both systems are a static electronic calculation done.

3.3.2 Sampling of the PES

Sampling the PES with regular MD is inherently inefficient and computationally expensive due to the fact that the adsorbate will tend to visit the lowest energy states with regular MD, so the probability of visiting all relevant meta-stable states and configurations of the PES is low. Therefore was metadynamics (MTD) implemented, presented in section 2.3, to increase the efficiency of sampling the PES. The goal was to find local minima, meta-stable states, that otherwise have low probability of being visited, but contribute non-negligible to the integral in (2.37). In other words, the adsorbed molecule prefers to visit low energy configurations during MD, and this search is enhanced with the help of MTD, the sampled configurations are more likely to be relevant, as the high energy configurations will barely be visited and if they are they have negligible impact on the final entropy.

The MD simulation of N_2@CHA$-SiO_2$was 50 ps. In the MTD of N_2@CHA$-SiO_2$, two CVs were used and were the distance between an atom in the zeolite and the center of mass of the N_2 with parameters $(h = 0.001, w = 0.05, t_G = 50)$ and $(h = 0.05, w = 0.1, t_G = 50)$. This was by any means an adequate choice of CVs, since N_2 was easily forced out of the zeolite pore and into another unit cell. This had the unfortunate consequence of the whole zeolite being translated and therefore the continued simulation was useless. Also, prior to the diffusion out of the cell, the CVs seem to have negligible influence as N_2 translated and rotated quite freely during regular MD. The sampling was deemed to be adequate based on the large exploration. New CVs were chosen for the other systems.

The CVs used for N_2@H-CHA and $[Cu(NH_3)_2]^+$@CHA were the cartesian coordinates of the center of mass (com) of the adsorbed molecule. For the linear molecule $[Cu(NH_3)_2]^+$, the Cu atom was assumed to be the com. As shortly mentioned in the theory section on MTD 2.3, the added gaussian bias potentials were not used after the MTD simulation to construct the free energy surface (FES) and therefore were the CVs chosen to only enhance the exploration of the PES. If a too large gaussian was added, meaning in the usual MTD context that it would cover a whole local minimum, the calculation of the PES would still capture the adsorption energy of this local minimum. If visited, of course. However, too large guassians added to V_{bias} led to visiting uninteresting, high energy, configurations. Therefore, the parameters height h, width w and update time step t_G were chosen carefully to slowly influence the dynamics.

MD production runs for N_2@H-CHA were done during the first 25 ps, of which the last 15 ps was with 0.5 fs time step as mentioned earlier. The remaining 30 ps of the combined trajectory was with MTD with the following set of parameters used $(h = 0.02, w = 0.05, t_G = 50)$.

In the case of $[Cu(NH_3)_2]^+$ in CHA, also additional metadynamics setups were used after the first MD production run of 30 ps. MTD with center of mass CVs (same as N_2@H-CHA), a production run of 5 ps with the set of parameters $(h = 0.02, w = 0.05, t_G = 50)$ was used and then was the resulting bias potential used with no further updates of the bias potential for a continuation run of 5 ps. A special probing MTD run was also implemented with $[Cu(NH_3)_2]^+$, due to its inability to visit a specific corner of the zeolite. A CV defined as the distance between the Cu atom of $[Cu(NH_3)_2]^+$ and a Si atom in the sparsely sampled corner with a gaussian added, pre-simulation, with $(h = 2, w = 0.01)$ 5 Å from the chosen Si atom. This was done to hinder the $[Cu(NH_3)_2]^+$ to diffuse too far away from the Si in the corner of interest. The $[Cu(NH_3)_2]^+$ was placed near the Si atom and the system was equilibrated shortly for 500 fs to avoid sampling unphysical structures, then a production run with metadynamics parameters $(h = 0.04, w = 0.05, t_G = 50)$ was simulated for 10 ps. The total simulation time for $[Cu(NH_3)_2]^+$@CHA was 50 ps.

3.3.3 Entropy with CPES

To evaluate the integral in eq. (2.37) and finally compute the entropy S^{CPES} in eq. (2.44), a PES on an evenly spaced grid was constructed using the sampled coordinates and their corresponding relative potential energy $U(\mathbf{r}, \mathbf{\Phi})$. N_2 is a linear molecule and $[Cu(NH_3)_2]^+$ was approximated as a linear molecule, and rotations around their linear axis were assumed to be negligible. Considering the NH_3 molecules in $[Cu(NH_3)_2]^+$, their electron density was almost invariant to rotations of the H atoms (homogenous). Therefore, only 2 rotational coordinates are required to (approximately) describe the full rotational space of the molecules so ψ in $\mathbf{\Phi}$, defined in eq. (2.37) can be omitted since its contribution to the integral is a factor 1. The other two angles to describe the rotations are here defined as θ and ϕ are

for spherical coordinates, see figure 3.3. $\theta \in [0, \pi)$ is defined from the positive z-axis to the negative z-axis, and $\phi \in [-\pi, \pi)$ is defined from the negative x-axis, $y < 0$, to the negative x-axis, $y > 0$, in the x-y plane. The vector $\vec{r}$ points from the center of mass to the N atom (for both N_2 and $[Cu(NH_3)_2]^+$) with the largest cartesian x-value.

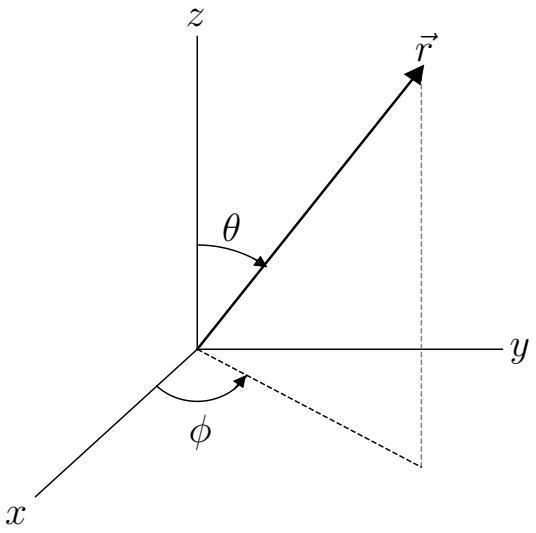

Figure 3.3: Spherical coordinates. The angles θ and ϕ describe with the radius $|\vec{r}| = r$ the point vector $\vec{r}$ points to. The angles are used to describe the molecule's rotation.

Using that both studied molecules are also invariant to permutation of the N atom, this local symmetry was implemented by changing the integration range for $\phi \in [-\pi/2, \pi/2]$, and taking this into account by changing the symmetry factor as $\sigma/2$ in eq. (2.37).

The periodicity of the rotations, $U(\boldsymbol{r}, \theta + \pi n, \phi + \pi m) = U(\boldsymbol{r}, \theta, \phi)$, where $n, m \in \mathbb{Z}$, were implemented in the interpolation by extending the sampled rotational coordinates by $\pi/6$ to each side of the rotational coordinates periods. Without this extension of the coordinates, a configuration with, for example, θ near 0 and another near π, and all other coordinates exactly the same, would still seem very far apart in the eyes of the interpolation algorithm. Regarding validation of the "model", calculations was done by ensuring its invariance to a shift in energy and also reproducing the result of the ideal gas for a flat energy surface.

With the interpolated PES grid, Simpson's rule implemented in the Scipy package [49] was used the integrate the PES. Points on the PES that were outside of the coordinate samples, i.e. could not be interpolated, were assumed to be a high energy section of the PES that could be, for example, very close to a zeolite atom. The energy of these points was set to 10 eV, which compared to the adsorption energies is very large and will give no contribution to the integral. A convergence test of the number of coordinate samples was done with a grid 100x100x100x20x20 for N_2 in

H-CHA, see fig. 4.10. For producing the final results, a grid as large as possible was used to interpolate the PES. The limitations were the fact the matrices in Python for large grids use several hundreds of GB RAM.A grid size of 101x101x101x25x25 was possible to implement without reaching the maximum memory limit of the compute nodes, which is the grid size used for the results for all three adsorption systems studied.

Spherical coordinates for the position $\boldsymbol{r}$ were considered, but were left due to the uneven spacing of the coordinate grid as well as difficulties implementing the periodicity and interpolation near $r = 0$.

3.4 Thermodynamic Integration (TI)

First is the general procedure to implement the method presented. Initially some results in methods original reference [1] reproduced to demonstrate that the implementation of the method is correct. This is done for the HF molecule at 2000 K and N_2 adsorbed in H-CHA at 200 K. Lastly is the new system $[Cu(NH_3)_2]^+$ adsorbed in CHA at 473 K studied.

3.4.1 Implementation

The studied structures were constructed and relaxed with a tolerance of 0.005 Å/eV. MD of the system and relevant subsystems, as the adsorbed molecule in gas-phase and clean substrate, were performed to study degrees of freedom and dynamics of the system(s).

From vibrational analysis of the relaxed structure using central finite differences could the force constants (eigenvalues) of the Hessian matrix $\boldsymbol{H^x}$ in eq. (2.62) be determined. For the zeolite systems the eigenvalues lower than a value were increased to the value. This was done to avoid divergence in the MD in accordance with [1]. The value increased to was 1-2 eV/Å depending on the system. The increase of eigenvalues can be viewed as the harmonic approximation where low energy modes as translations and rotations have increased energy. Imaginary, soft, modes were discarded. With the ground state electronic energy and the eigenfrequencies was the classical harmonic Helmholtz free energy $A_{0,\boldsymbol{x}}$ calculated with eqs. (2.63) and (2.64).

The procedure to calculate the ensemble averages $\langle V_1 - V_{0,\boldsymbol{q}} \rangle_\lambda$ and $\langle V_{0,\boldsymbol{q}} - V_{0,\boldsymbol{x}} \rangle_\lambda$ to determine $\Delta A_{0,\boldsymbol{q} \longrightarrow 1}$ and $\Delta A_{0,\boldsymbol{x} \longrightarrow 0,\boldsymbol{x}}$, is in principle the same, although there were some practical differences. For both averages, the Andersen thermostat was used. The reason for using the Andersen thermostat is because the harmonic MD program only has that thermostat, and to avoid any discrepancies between the hMD program and VASP's MD, Andersen was used in VASP as well, which is also how TI is implemented in the original work [1]. The collision probability per time step parameter differed for each case and is stated in the corresponding section below.

For the correction term for the transformation from the system harmonic in $\boldsymbol{q}$ to the fully interacting system 1 (DFT), VASP was used and other than the usual input parameters for MD, a parameter selecting the λ-value must be supplied as well. The Hessian matrix from the first step, vibrational analysis, and the internal coordinates $\boldsymbol{q}$ were also required. The average $\langle V_1 - V_{0,\boldsymbol{q}} \rangle_\lambda$ was calculated for a discrete set of λ-values. In some cases, the average changed quickly with increasing λ, which required high grid density for λ near 1.

To calculate the correction term $\Delta A_{0,\boldsymbol{x}\longrightarrow 0,\boldsymbol{q}}$ the harmonic molecular dynamics (hMD) program was used instead of VASP. Other than that there were only system specific differences. As mentioned in the introduction of this chapter, various tools to construct the Hessian matrix, simplifying the process of constructing internal coordinates and harmonic MD were provided by Bučko [1].

All integrals were computed using Simpson's rule. Simpson's rule requires an odd number of points, to generate an even number of intervals, since Simpson's rule fits a second degree polynomial, which requires 3 points. In the cases of having an even number of points, the trapeziodal rule is used for the last interval. This was chosen due to large changes near $\lambda = 1$, which fitting a second degree polynomial to might lead to large errors when the points are unevenly spaced (which they are in the implementation here), also known as overfitting. Although, a possible solution to this would be to sample λ more near $\lambda = 1$.

The statistical errors were estimated for each average $\langle ... \rangle_\lambda$ and the integral (correction terms). For the average, the standard error $\epsilon = \sigma/\sqrt{N}$, where σ is the standard deviation and N the number of samples, was estimated using a block averaging method to eliminate time correlation [16]. The standard error of the integral I was then determined with the error propagation estimation [1]

$$\epsilon_I = \sqrt{\sum_\lambda \left(\frac{\partial I}{\partial f_\lambda} \epsilon_{f_\lambda} \right)^2} \tag{3.1}$$

where $f_\lambda = \langle ... \rangle_\lambda$ and ϵ_{f_λ} is the corresponding estimated standard error, found with the above mentioned block averaging method. A step of $\Delta f_\lambda = 0.001$ and central finite differences was used for the numerical derivative of $\frac{\partial I}{\partial f_\lambda}$.

3.4.2 HF molecule

The gas phase HF molecule was set up in a unit cell with edge length of 15 Å. The internal coordinate $\boldsymbol{q}$ used for HF was the bond length. The correction term $\Delta A_{0,\boldsymbol{q}\longrightarrow 1}$ was calculated with VASP's MD at temperature 2000 K, with an Andersen thermostat probability of 0.05 and timestep 0.25 fs. The van der Waals correction D2-method of Grimme was used and a SCF convergence criteria 10^{-6} eV. The system was equilibrated for 1.25 ps and production runs to calculate $\langle V_1 - V_{0,\boldsymbol{q}} \rangle_\lambda$ varied between 5 and 16.25 ps, depending on at which speed the average converged. The DFT potential to calculate the exact semi-analytical reference $\Delta A^{\text{ref}}_{0,\boldsymbol{q}\longrightarrow 1}$ was cal-

culated by incrementing the distance between HF from 0.5 to 2 Å with a stepsize of 0.01 Å and calculating the static electronic energy at each step/structure. The parameters for the MD were chosen to be similar to the parameters used in the TI reference article [1]. With the harmonic frequency from the vibrational analysis A_{vib} was calculated, and the final anharmonic vibrational entropy contribution to the free energy could be found.

3.4.3 N_2 adsorbed in H-CHA

To calculate the Helmholtz free energy of adsorption, A_1 for N_2 in H-CHA, the clean H-CHA and N_2 in gas phase are required. For gas phase N_2 , vibrations were approximated as harmonic, eq. (2.26), and rotation and translation with the rigid rotor, eq. (2.24), and ideal gas approximations, eq. (2.22), respectively. For gas phase diatomic molecules the anharmonic contribution is small, therefore the harmonic approximation is reasonable [1]. The (Helmholtz) free energy of adsorption is then

$$\Delta A = A_{1,\mathrm{N_2@H-CHA}} - A_{1,\mathrm{H-CHA}} - A_{1,\mathrm{N_2}} \tag{3.2}$$

where N_2@H-CHA denotes N_2 adsorbed in H-CHA. The internal coordinates were set up as described in section 2.6.3 regarding internal coordinates $\boldsymbol{q}$. For the N_2 molecule, the bond length was used. For the H-CHA substrate, interatomic distances to all atoms in the three coordination spheres were used, except for the special Brønstedt site, which is treated as a flexible site. Therefore, for the hydrogen atom, the internal coordinates were the bond length to the oxygen it is bound to, the angle to the atoms that oxygen is bound to, with the oxygen as apex, and finally the smallest torsion angle, in relaxed structure, to one oxygen bound to Al. For the internal coordinates describing the translations and rotations of N_2 in H-CHA, coordination number CN was used for all N-Si and N-Al pairs, with reference distance 3.5 Å, which is approximately the sum of their vdW radius. Also, at the reference distance the N_2 is in the center of the zeolite cage. The CN coordinates influence the involved atoms when they are within the vdW interaction range. The system's invariance of permutation of N atoms was implemented with a symmetric linear combination of the CN coordinates between one substrate atom and both N atoms. The eigenvalues of the clean H-CHA were increased to 1 eV/Å and for N_2@H-CHA they were increased to 2 eV/Å.

The temperature 200 K was realized with the Andersen thermostat with a collision probability of 0.02. For all systems, i.e. for all values of λ, the equilibration time was 5 ps and the length of production runs was in the range of 37 to 115 ps, depending on how quick convergences were. The time step for the MD for the $\Delta A_{0,\boldsymbol{q}\longrightarrow 1}$ term was 1 fs and the total production run length for all λ combined was for N_2@H-CHA 450 ps and for the empty H-CHA 183 ps, while the timestep was 0.5 fs in hMD for the $\Delta A_{0,\boldsymbol{x}\longrightarrow 0,\boldsymbol{q}}$ with production run length for N_2@H-CHA of 935 ps and the clean H-CHA 315 ps. The vdW correction D2-method by Grimme was used to be able to reproduce the results in the reference TI article [1].

To compare the result with the reference [1], where the final resulting adsorption free energy was presented as Gibbs free energy, the Helmholtz free energy for the gas molecule A_{1,N_2} was required to be transformed to Gibbs free energy $G_{1,N_2} = A_{1,N_2} + \frac{7}{2}k_BT$, where the latter is the heat capacity contribution the enthalpy. The PV term of both zeolite structures N_2@H-CHA and H-CHA were assumed to cancel [1].

3.4.4 $[Cu(NH_3)_2]^+$ adsorbed in CHA

The Helmholtz free energy of adsorption was calculated as in the previous section with N_2 in H-CHA. The internal coordinates for $[Cu(NH_3)_2]^+$ were bond lengths for all atoms, angles between the hydrogen atoms, and interatomic distances from Cu to all H, and lastly an interatomic distance between the N atoms. The distance between the N atoms was required to keep the molecule linear, since the angle between the atoms could not be used due to that it is larger than 165°. All substrate internal coordinates were described by interatomic distances to all atoms in the first three coordination spheres for each atom in the substrate. The coordination number CN coordinates to describe the translation and rotation of $[Cu(NH_3)_2]^+$ were for the N atoms set up as for N_2 in H-CHA in the previous section, with the linear combination of CNs to account for the symmetry. CNs were also used for all Cu-Si and Cu-Al pairs. The hydrogen atoms in $[Cu(NH_3)_2]^+$ were omitted from the translational and rotational description of the molecule in the zeolite, since they always follow the N atoms. The eigenvalues for both systems were increased to 2 eV/Å, if lower than this value, i.e. the harmonic approximation.

The temperature 473 K was realized with the Andersen probability of 0.02. The time step for the MD for the $\Delta A_{0,\boldsymbol{q}\longrightarrow 1}$ terms was 1 fs for both the full system $[Cu(NH_3)_2]^+$@CHA and the clean CHA with a total production run time of 440 ps and 69 ps, respectively. The timestep was 0.5 fs in hMD for the $\Delta A_{0,\boldsymbol{x}\longrightarrow 0,\boldsymbol{q}}$ and the production runs for $[Cu(NH_3)_2]^+$@CHA were 760 ps and for the clean CHA 225 ps. For all correction terms and each λ, 5 fs was deemed to be enough equilibration time. The production run length varied in the range of 27 ps to 230 ps depending on how quickly the average converged. Note, the vdW correction D3-method by Grimme was used, in similarity with the CPES simulations.

4
Results

First the results from CPES are presented, including the analysis of the fixed and dynamic framework of the zeolite, the sampling of the PES and finally the resulting entropies. Then, TI is presented with the reproduced cases with HF molecule and N_2 in H-CHA, and next results for $[Cu(NH_3)_2]^+$ in CHA are shown. Lastly, the resulting entropies from CPES and TI with each other and experimental values.

4.1 CPES

4.1.1 Framework analysis

The potential energy of MD simulations of the fully dynamic, no fixed atoms, zeolite systems N_2 in H-CHA and $[Cu(NH_3)_2]^+$ in CHA is seen in figure 4.1 to the left respective right. It is clearly difficult to distinguish between vibrations and the translational and rotational relative potential energy. The overall appearance and features of the PES are more clearly seen in figure 4.2 where the zeolite frame is fixed. For N_2 especially is the high frequency vibrational energy seen superimposed on the energy of the slower dynamics of the molecule moving inside the zeolite. These vibrations of N_2 could, with some data processing, be filtered out. However, as seen for $[Cu(NH_3)_2]^+$ (right) this is not as simple because it is not as obvious what corresponds to vibrations or translation/rotation of the $[Cu(NH_3)_2]^+$ molecule.

Lastly, the implemented procedure to calculate the PES from the MD simulation is seen in figure 4.3. Here, as described in section 3.3.1, the adsorbed molecule is removed from the zeolite and their static energies are computed separately and subtracted from the total system energy. In the case of N_2 in H-CHA (left) the vibrations are clearly eliminated and at this particular snapshot of the MD trajectory an energy peak is seen which corresponds to the N_2 hitting the inside wall of the H-CHA. In the case of $[Cu(NH_3)_2]^+$ (right) the dynamics are faster than for N_2 and some variations might correspond to vibrations but compared to $[Cu(NH_3)_2]^+$ in a fixed zeolite, seen in figure 4.2, the energy is much smoother. Also, from this analysis it was concluded that to capture the comparable slow translations and rotations it is sufficient to compute the static energies for the adsorbate and substrate separately every fourth step, i.e. every 4 fs for these simulations with 1 fs time step.

The dynamic method to compute the PES also makes it possible to capture the dynamics of the zeolite framework and its interaction with the adsorbed molecule,

which can influence diffusion and adsorption energy as mentioned in 3.3.1. The behavior of N_2 in H-CHA was also studied and the distance traveled by the adsorbed N_2 in a fixed framework and dynamic framework is seen in figure 4.4. N_2 in the dynamic framework moves about half as slowly compared to in the fixed framework. Studying the MD trajectories, in the fixed framework the adsorbed N_2 bounces more or less elastically on the inside walls, while in the dynamic framework the collisions with the walls seem more inelastic and the N_2 therefore loses kinetic energy. Although the analysis of the difference between a fixed and a dynamic framework can be more thorough, this result gives the indication that there might be some differences.

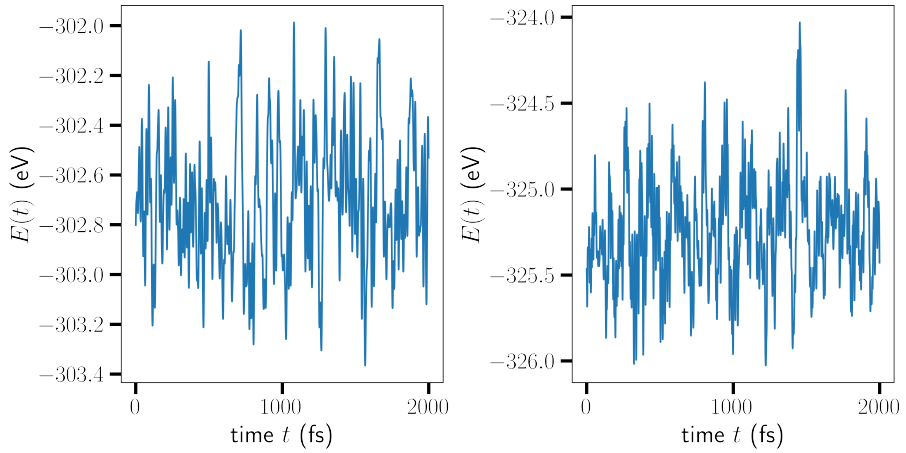

Figure 4.1: Total system energy of the full dynamic zeolite in an MD run. To the left N_2 in H-CHA and to the right $[Cu(NH_3)_2]^+$ in CHA.

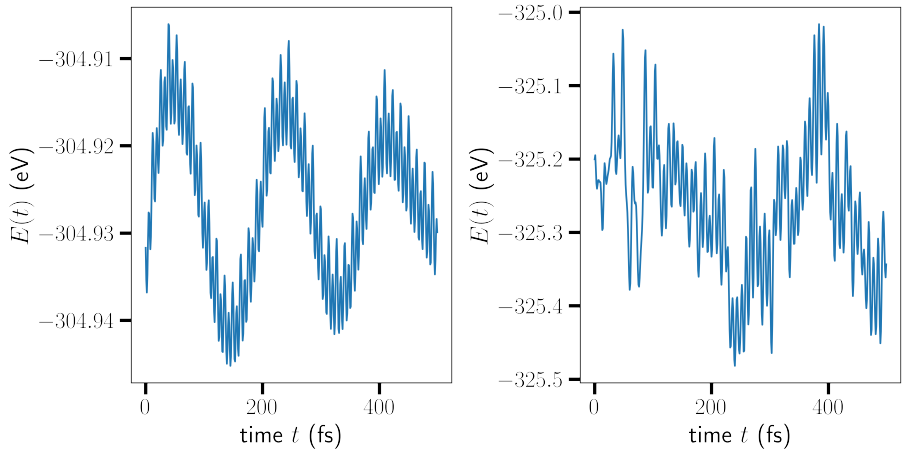

Figure 4.2: The energy in an MD with fixed zeolite framework. The energy consists therefore of the translational and rotational PES of the N_2 (left) and $[Cu(NH_3)_2]^+$ (right) as well as their vibrations.

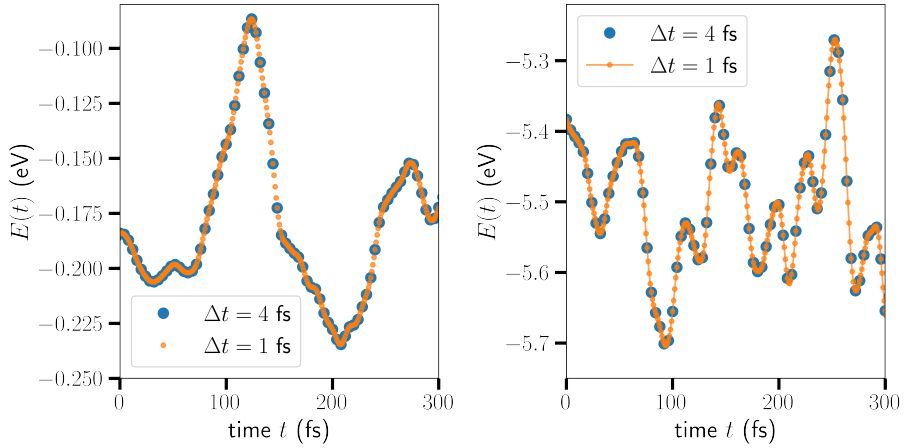

Figure 4.3: The energy in an MD with dynamic zeolite framework and the vibrations of the molecule and zeolite subtracted. N_2 to the left and $[Cu(NH_3)_2]^+$ to the right. Two different Δt are shown, 1 fs and 4 fs. It was concluded that recalculating every 4th step is enough to describe the slow, relative to vibrations, translations and rotations.

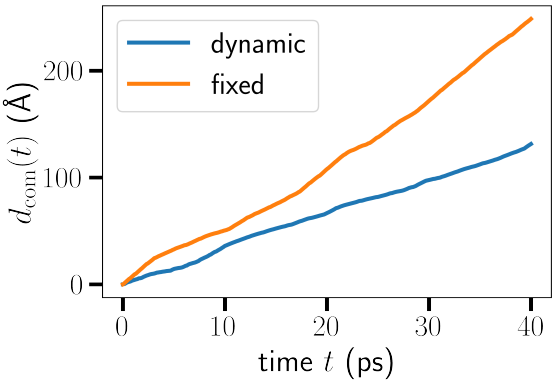

Figure 4.4: The distance traveled by the center of mass (com) of the N_2 , $d_{com}(t)$, at time t in a zeolite with fixed framework and dynamic framework.

4.1.2 Sampling

The trajectories of the production runs of N_2@CHA−SiO_2, N_2@H-CHA and $[Cu(NH_3)_2]^+$@CHA are seen in figs. 4.5, 4.6 and 4.7, respectively. Each figure consists of three subfigures, where the upper is the energy $U(\mathbf{r}, \mathbf{\Phi})$ as defined in eq. (2.38). Since the static structures only are recalculated every 4 fs, only these steps are therefore plotted of the trajectory. In the middle subfigure the cartesian coordinates (x, y, z) of the center of mass of the adsorbed molecule (N_2 or $[Cu(NH_3)_2]^+$), describing the translation, is seen. In the lower subfigure the generalized angle coordinate θ/π and $\phi/(2\pi)$ is seen. Note that since $\theta \in [0, \pi)$ gives $\theta/\pi \in [0, 1)$ and for $\phi \in [-\pi, \pi)$, when the symmetry is also accounted for, gives $\phi/(2\pi) \in [-0.25, 0.25)$, which is seen in the lower subfigures. We see that for both N_2 and $[Cu(NH_3)_2]^+$ the energy fluctuates substantially when they diffuse inside the zeolite. Further, for N_2 in both CHA−SiO_2 and H-CHA, it is clear that the molecule visits many

translational and rotational configurations, especially considering the lower subfigures where one can see the frequent rotation. Note that the reason the rotational coordinates are discontinuous is due to the periodicity.

For $[Cu(NH_3)_2]^+$ however, the rotations of the molecule are limited compared to N_2. At first, this might seem to be problematic since the sampling of the full PES is incomplete. But, as discussed earlier, it is the lowest energy $U(\mathbf{r}, \mathbf{\Phi})$ configurations that are of most interest because they contribute most to the integral in CPES, see eq. (2.37). Especially when ϕ deviates from its most common value, we can see that the energy increases, which is most apparent between 30 and 40 ps in fig. 4.7. Although there is a risk that essential local energy minima are missed, due to the long simulation of 50 ps in combination with various metadynamics schemes, the results can be seen with at least some confidence.

The sampling result of $[Cu(NH_3)_2]^+$ also hints at the fact that translation and rotation are closely connected and dependent on each other, hence the importance to describe their relation adequately. Also, at the difficulty to find the entropy of large adsorbed molecules that have hindered rotations depending on where in the zeolite it is. For the smaller molecule studied, N_2 , this is not as prominent.

The sampled coordinates are also visualized as distributions for each coordinate on the diagonal and as joint distributions for each pair of coordinates for N_2@H-CHA and $[Cu(NH_3)_2]^+$@CHA , by so called corner-plots [17], in fig. 4.8 and 4.9, respectively. N_2@CHA$-SiO_2$ is omitted since it is very similar to N_2@H-CHA. Overall, the distribution for N_2 is more evenly spread than for $[Cu(NH_3)_2]^+$. Especially the sampling of ϕ differs between N_2 and $[Cu(NH_3)_2]^+$, which also shows in the joint distribution of θ and ϕ where the distribution is narrow. From this we see that $[Cu(NH_3)_2]^+$ prefers a specific orientation.

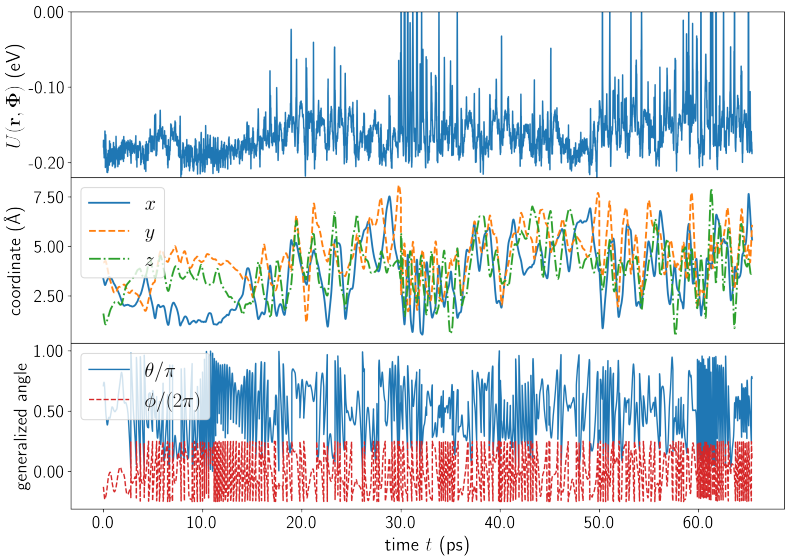

Figure 4.5: The production run trajectory of N_2@CHA−SiO_2. The upper figure shows the adsorption energy $U(\mathbf{r}, \mathbf{\Phi})$, the middle the corresponding cartesian coordinates (x, y, z) of the center of mass, and the lower figure the corresponding generalized rotational angles θ/π and $\phi/(2\pi)$.

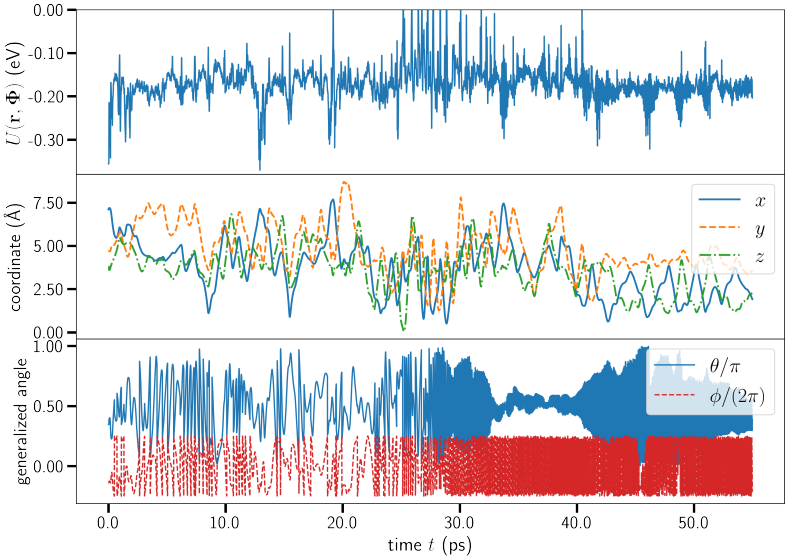

Figure 4.6: The production run trajectory of N_2@H-CHA. The upper figure shows the adsorption energy $U(\mathbf{r}, \mathbf{\Phi})$, the middle the corresponding cartesian coordinates (x, y, z) of the center of mass, and the lower figure the corresponding generalized rotational angles θ/π and $\phi/(2\pi)$.

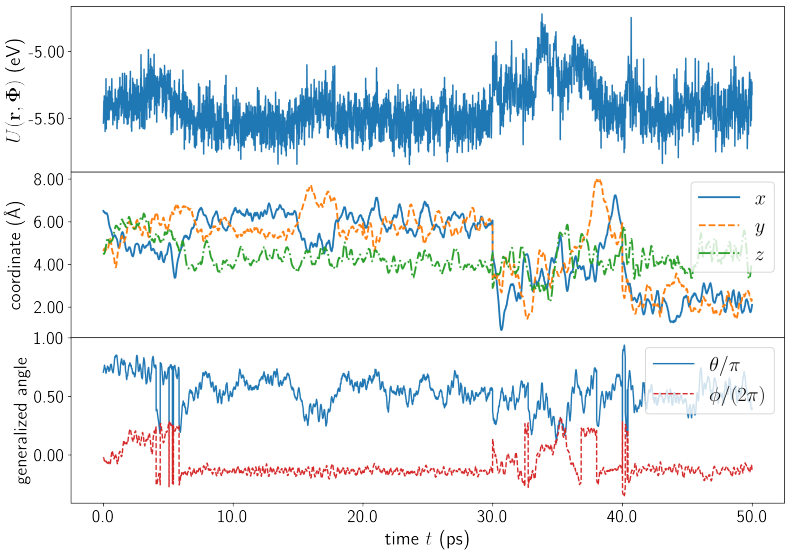

Figure 4.7: The production run trajectory of $[Cu(NH_3)_2]^+$@CHA. The upper figure shows the adsorption energy $U(\mathbf{r}, \mathbf{\Phi})$, the middle the corresponding cartesian coordinates (x, y, z) of the center of mass, and the lower figure the corresponding generalized rotational angles θ/π and $\phi/(2\pi)$.

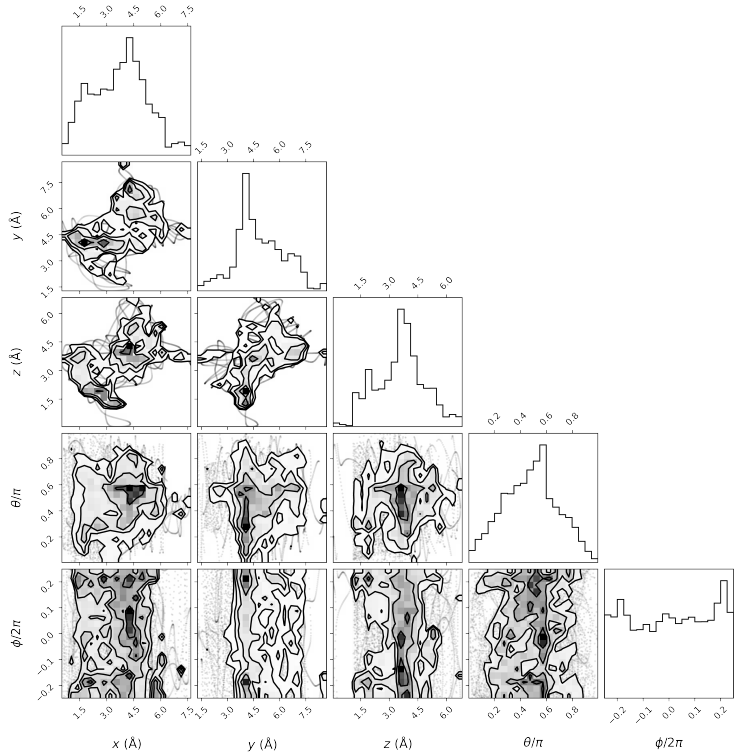

Figure 4.8: Distributions of the sampled coordinates for N_2 on the diagonal and below are pair-wise joint distributions.

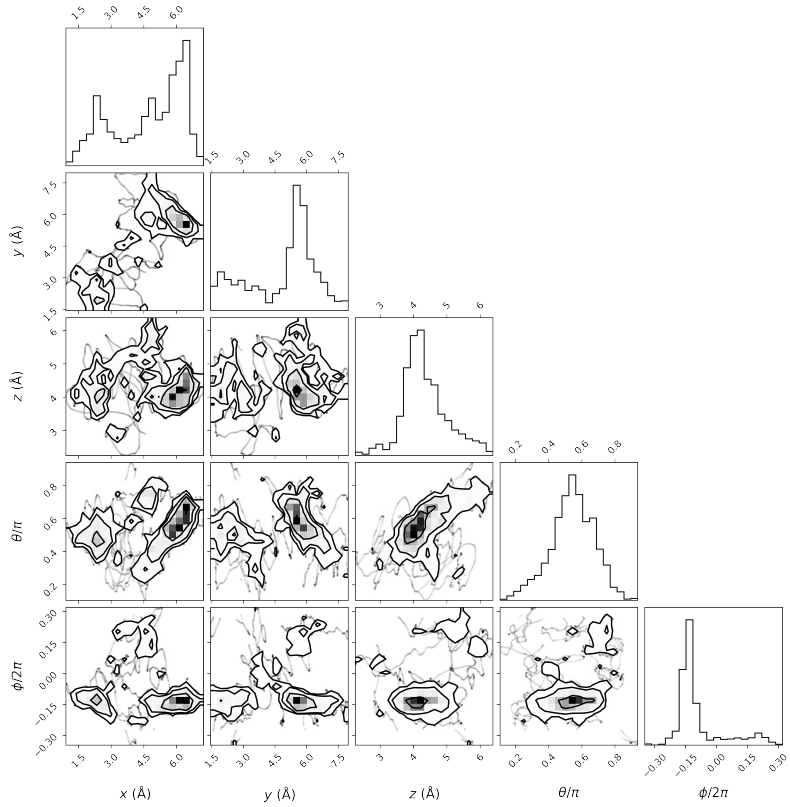

Figure 4.9: Distributions of the sampled coordinates for $[Cu(NH_3)_2]^+$ on the diagonal and below are pair-wise joint distributions. Even with MTD is the hindered rotation of the large $[Cu(NH_3)_2]^+$ clearly visible for ψ, where most of the time the molecule is stuck at one rotational configuration.

4.1.3 Entropy

Prior to the construction of the PES for the studied systems the sampled data were extended with duplicates, which was done to ensure the periodicity condition in the interpolation as described in section 3.3.3. An important note is that the addition of the periodic data points does not add any new information.

At the extension of the sampled data, the number of points for N_2@CHA$-SiO_2$ increased from 16350 to 24822, N_2@H-CHA from 13750 to 21216 and $[Cu(NH_3)_2]^+$@CHA from 12500 to 15232. A convergence test with respect to the number of data points used in the interpolation of the PES for N_2@H-CHA is seen in fig. 4.10, using the extended data set, with a grid consisting of 110 points for cartesian coordinates and 20 points for angle coordinates, i.e. 110x110x110x20x20, at the temperature 473 K. The points were selected as every one, second, third, fourth, and so on, to ensure an even distribution of the selected data. From the convergence test it was concluded that at least 10000 data points of the extended set are sufficient, and valid for systems with the same coordinates as N_2, which $[Cu(NH_3)_2]^+$ also has.

In the subsequent calculations of entropy, another grid size of 101x101x101x25x25 was used due to computational practicalities and a higher resolution in the angle coordinates. This grid was deemed to be a good balance between computational expense and accuracy, noting that the entropy for N_2@H-CHA was exactly the same for both grids, when all data points were used at 473 K.

In fig. 4.11 is $TS^{\mathrm{CPES}}_{\mathrm{trans,rot,linear}}$ for different temperatures shown for the three studied zeolite systems, in other words merely the translational and rotational adsorbate entropy, see eq. (2.45). At low temperatures N_2@CHA$-SiO_2$ has slightly larger entropy than N_2@H-CHA but the difference becomes negligible as the temperature increase. This can be interpreted as that the PES is fairly similar for both N_2 systems, but the interaction with H-CHA is slightly stronger.For the $[Cu(NH_3)_2]^+$ system the difference is more significant. $[Cu(NH_3)_2]^+$ is a larger and heavier molecule than N_2 , and at low temperatures the entropy is lower for $[Cu(NH_3)_2]^+$ than for the N_2 systems. Interestingly, when the temperature increase $[Cu(NH_3)_2]^+$@CHA pass the N_2 systems and have higher absolute entropy.

The resulting entropies are also seen in fig. 4.12, where to the left the adsorption entropy, $T(S^{\mathrm{CPES}} - S^{\mathrm{gas}})$, at 101.325 kPa is shown and to the left γ, defined in eq. (2.46). Once again a slight difference between the N_2 systems is seen at lower temperatures but converges to the same value, which at high temperatures can be interpreted as that the PES plays an insignificant role and N_2 behaves as a gas molecule but constrained in the zeolite cage, which is a smaller volume than for an ideal gas at 101.325 kPa. Compared to the N_2 systems, the $[Cu(NH_3)_2]^+$ complex lose more entropy at adsorption both in absolute terms and in relative terms, which is because the translations and rotations of $[Cu(NH_3)_2]^+$ are much more limited than for N_2 which was seen directly in figs. 4.7 and 4.9. Another interesting observation is that even at 600 K, $[Cu(NH_3)_2]^+$ is quite far from reaching a convergence of γ as we see for the N_2 systems, in other words, the PES affects the $[Cu(NH_3)_2]^+$ systems

more and to judge from the sampling the PES is probably more intricate.

Lastly, the CPES method is based on exploring the PES and in particular finding as many minima and their surroundings as possible. Visualizing a 5D PES is very difficult and thus has been omitted in this thesis to avoid showing any misleading results. However, the figs 4.5, 4.6 and 4.7 shows well the translational and rotational configurations and their corresponding relative potential energy $U(\mathbf{r}, \mathbf{\Phi})$ and as described in section 3.3.3 unsampled region were approximated to be 10 eV, which in essence means an extremely low probability that that region is visited by the adsorbed molecule.

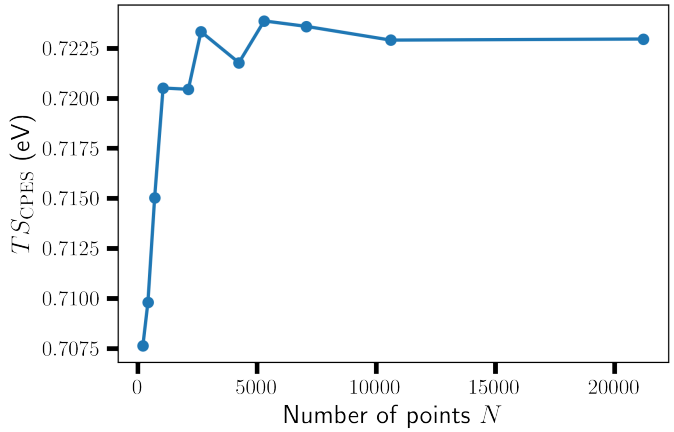

Figure 4.10: Convergence of S_{CPES} for N_2@H-CHA at $T = 473$ K.

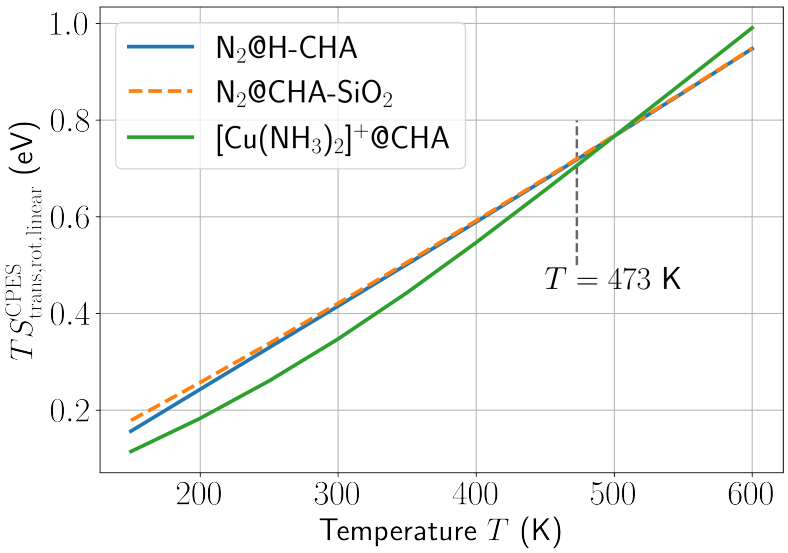

Figure 4.11: $TS^{\mathrm{CPES}}_{\mathrm{trans,rot,linear}}$ vs T for N_2@H-CHA, N_2@CHA$-SiO_2$ and $[Cu(NH_3)_2]^+$@CHA.

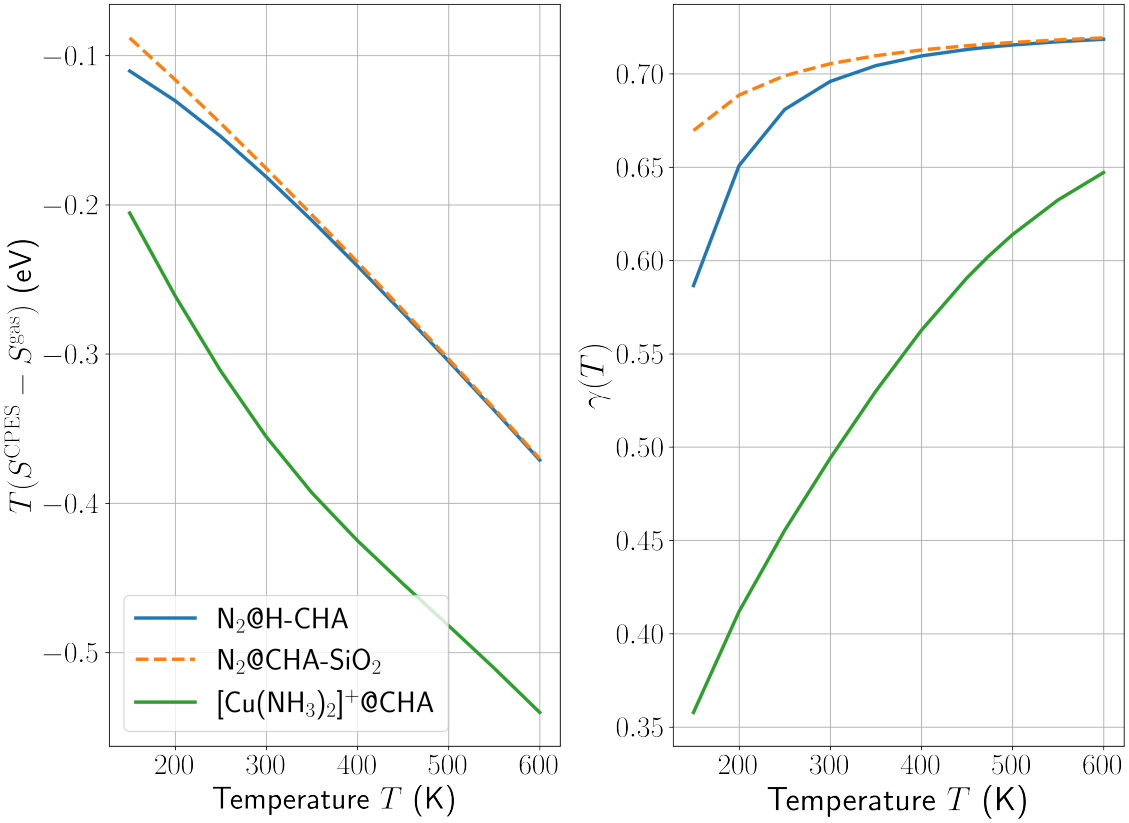

Figure 4.12: $T\Delta S$ and γ vs temperature T at 101.325 kPa for N_2@H-CHA, N_2@CHA−SiO_2 and $[Cu(NH_3)_2]^+$@CHA.

4.2 TI

4.2.1 HF molecule

The bond length of the relaxed molecule was found to be $R_0 = 0.938$ Å and from the subsequent vibrational analysis with central finite differences, the vibrational angular frequency $\omega = 456.28$ THz was determined, which results in $A_{\mathrm{vib}} = 95.71$ meV. With the mass of tritium used for the hydrogen atom, the force constant is $C = 55.905$ eV Å^{-2} for the harmonic potential

$$V_{0,\boldsymbol{q}}(R) = V_{0\boldsymbol{q}}(R_0) + \frac{1}{2}C(R - R_0)^2. \tag{4.1}$$

The harmonic potential $V_{0,\boldsymbol{q}}(R)$ and the true potential V_1 are seen in fig. 4.13 as well as the probability density of the bond length when the system is driven by either only $V_{0,\boldsymbol{q}}(R)$ or V_1. In the figure is also the HF molecule is seen, where fluoride is the larger green atom and hydrogen is the smaller white atom. The anharmonicity of the bond is clearly seen in the difference in the potentials. The effect of the steeper V_1 for $R < R_0$ while also flatter for $R > R_0$ compared to $V_{0,\boldsymbol{q}}$ is seen in the slight shift to larger R in the probability density p_1 in comparison to $p_{0,\boldsymbol{q}}$.

The average $\langle V_1 - V_{0,\boldsymbol{q}} \rangle_\lambda$ sampled from MD for $\lambda = 0, 0.25, 0.5, 0.75, 1$ is seen in fig.

4.14 as the orange dots with the statistical error ϵ_{f_λ} and the exact semi-analytical reference $\langle V_1 - V_{0,\boldsymbol{q}} \rangle_\lambda^{\text{ref}}$ as the blue line, which is calculated using the sampled V_1 potential and eq. (2.70). The blue area visualize the integral of $\langle V_1 - V_{0,\boldsymbol{q}} \rangle_\lambda$ and is equal to the correction term $\Delta A_{0,\boldsymbol{q} \longrightarrow 1}$. e

Further, the reference correction term $A^{\text{ref}}_{0,\boldsymbol{q} \longrightarrow 1} = -7.6$ meV, calculated with eq. (2.69). Integration of the sampled $\langle V_1 - V_{0,\boldsymbol{q}} \rangle_\lambda$ yields $\Delta A_{0,\boldsymbol{q} \longrightarrow 1} = -7.8 \pm 0.6$ meV, which is close and within the error margin of the true value $\Delta A^{\text{ref}}_{0,\boldsymbol{q} \longrightarrow 1} = -7.6$ meV. Since $A_{0,\boldsymbol{x} \longrightarrow 0,\boldsymbol{q}} = 0$, this results in a reference value of 88.17 meV to the sampled value $A_1 - A_{\text{el}}(\boldsymbol{x}_0) = 87.95 \pm 0.58$ meV. While $A_{\text{el}}(\boldsymbol{x}_0) = -7.8885$ eV, the entropy contribution to the Helmholtz free energy is small and the anharmonic correction even smaller.

The results agree well with the TI reference article, where they found $R_0 = 0.938$ Å and $C = 56.157$ eV Å^{-2}, but more importantly, their $\Delta A^{\text{ref}}_{0,\boldsymbol{q} \longrightarrow 1} = -7.6$ meV and $\Delta A_{0,\boldsymbol{q} \longrightarrow 1} = -8.1 \pm 0.5$ meV [1]. This demonstrates the correct implementation of the TI method.

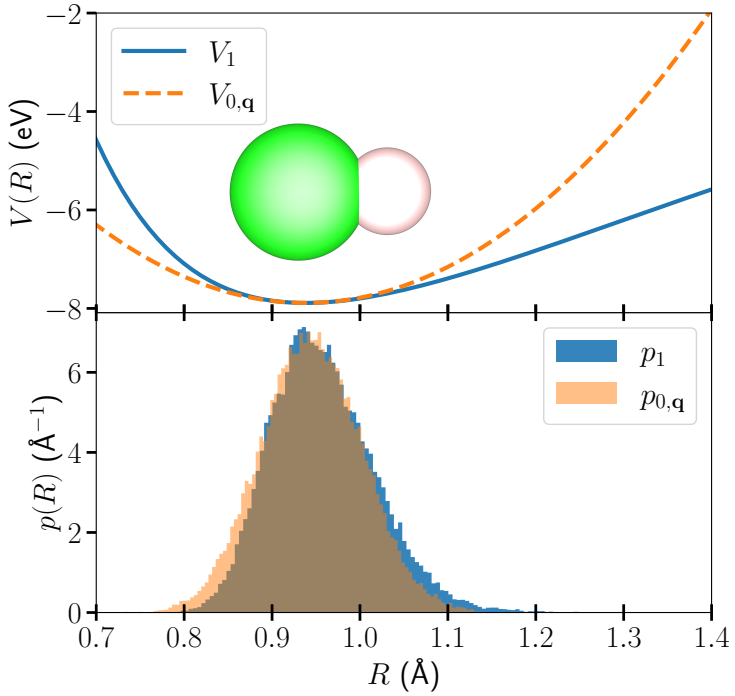

Figure 4.13: (top): Potential energy as a function of bond length of HF for V_1 (DFT) and the harmonic approximation $V_{0,\boldsymbol{q}}$. (bottom): The probability density $p(R)$ of the bond length for the system driven by V_1 and $V_{0,\boldsymbol{q}}$ at 2000 K.

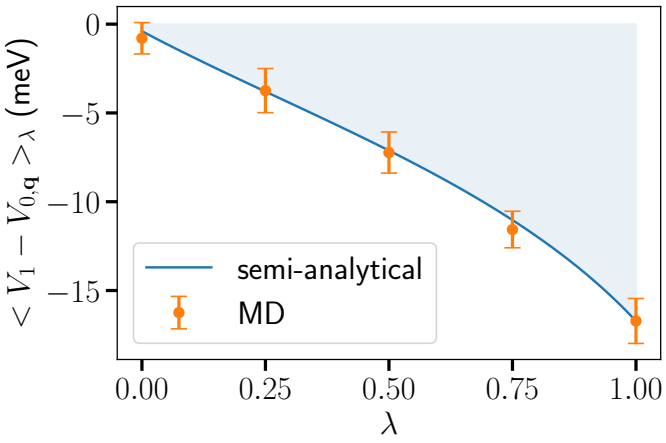

Figure 4.14: Result of $\langle V_1 - V_{0,\boldsymbol{q}} \rangle_\lambda$ from MD compared to the exact semi-analytical solution.

4.2.2 N_2 adsorbed in H-CHA

The dynamics of the system driven by one of the potentials $V_{0,\boldsymbol{x}}, V_{0,\boldsymbol{q}}, V_1$ at a time is visualized in fig. 4.15 as a radial distribution function (RDF) for the two N atoms constituting N_2 to the H atom, of the Brønstedt site, in H-CHA. The RDF tells how the number density of atoms varies with the radial distance from a reference position, in this case the $\text{RDF}_{\text{N-H}}$ describes at which distances the N atoms are from H. With $V_{0,\boldsymbol{x}}$, the N atoms barely leave their distances of 2 and 3 Å to the H atom and as the line (blue) between the peaks is zero this shows that no rotations are present. With $V_{0,\boldsymbol{q}}$ and subsequently V_1, the RDF is increasingly smeared out, showing that N_2 is allowed to diffuse around in the cage more. The RDF demonstrates how the harmonic approximation fails to capture the true dynamics, and consequently, the true thermodynamic properties of the system.

The averages $\langle V_{0,\boldsymbol{q}} - V_{0,\boldsymbol{x}} \rangle_\lambda$ and $\langle V_1 - V_{0,\boldsymbol{q}} \rangle_\lambda$ required to compute the free energy corrections for N_2 @H-CHA is seen in figs. 4.16 and 4.17. The averages from MD for the various λ are plotted as orange dots with error bars showing the statistical error ϵ_{f_λ}. For this system, there is no semi-analytical solution as there is for the HF molecule, but a linear interpolation is seen as the dotted blue line to help guide the eyes and also a light blue area serving the purpose to visualize the integral. As λ approaches 1, the average quickly changes and the higher sampling density near $\lambda = 1$ is clearly required. Also, the statistical error is not insignificant for larger λ, which demonstrates the time consuming and computationally expensive task to reach convergence.

Similarly, $\langle V_{0,\boldsymbol{q}} - V_{0,\boldsymbol{x}} \rangle_\lambda$ and $\langle V_1 - V_{0,\boldsymbol{q}} \rangle_\lambda$ for the empty H-CHA is seen in fig. 4.18. The change in $\langle ... \rangle_\lambda$ is not as dramatic for this system and the errors are smaller than for the system with N_2 adsorbed.

After calculating $A_1 = A_{0,\boldsymbol{x}} + \Delta A_{0,\boldsymbol{x} \longrightarrow 0,\boldsymbol{q}} + \Delta A_{0,\boldsymbol{q} \longrightarrow 1}$ for both N_2@H-CHA and the empty H-CHA, and approximating A_1 as A_0 for gas phase N_2 , i.e. as an ideal gas at

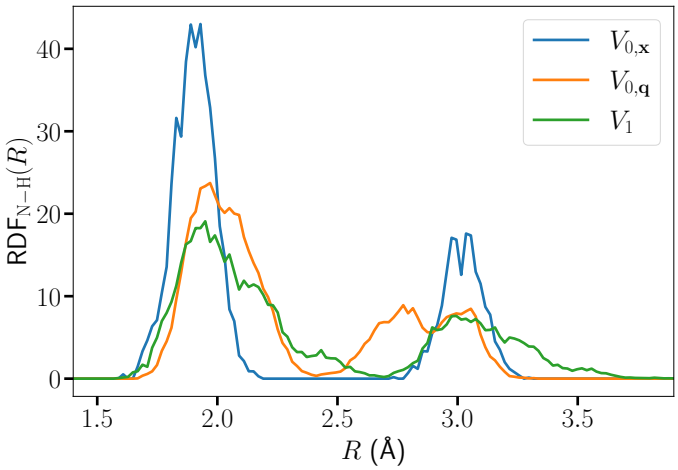

Figure 4.15: RDF for N atoms to H. The larger movement of the N atoms is visible when the system is driven by DFT (V_1) compared to the harmonic forcefields $V_{0,\boldsymbol{q}}$ and $V_{0,\boldsymbol{x}}$.

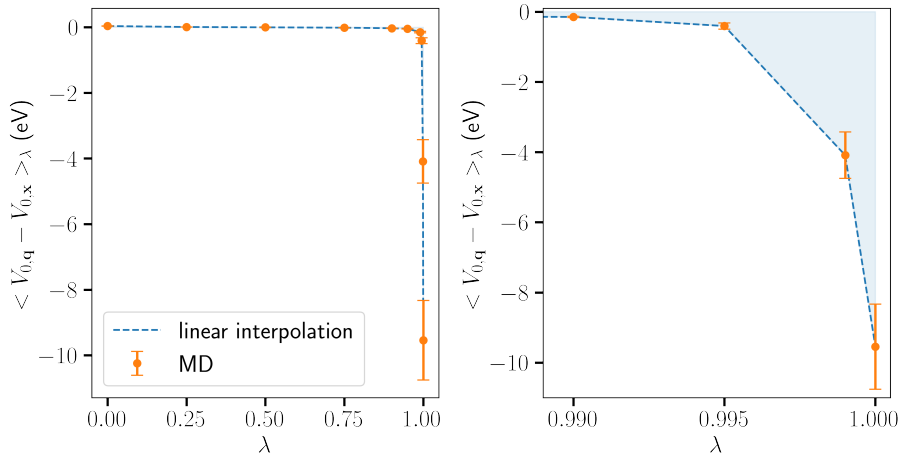

Figure 4.16: Averages $\langle V_{0,\boldsymbol{q}} - V_{0,\boldsymbol{x}} \rangle_\lambda$ to compute the forcefield-forcefield transformation $\Delta A_{0,\boldsymbol{x} \longrightarrow 0,\boldsymbol{q}}$ for N_2 in H-CHA.

101.325 kPa, free translator and rigid rotator, $\Delta A_{\mathrm{ads}} = A_{1,\mathrm{N_2@H-CHA}} - A_{1,\mathrm{H-CHA}} - A_{0,\mathrm{N_2}}$ is calculated. All relevant terms that contribute are seen in table 4.2 and can be compared with the same results from the TI reference article in table 4.3. The result yields $\Delta A_{\mathrm{ads}} = 0.00787 \pm 0.006$ eV. In this case, Helmholtz free energy can easily be rewritten as Gibbs free energy by assuming the pV term of the two zeolite systems cancel and only a contribution of $k_B T$ from gas phase N_2 is therefore only required to switch from canonical ensemble to Gibbs ensemble [10], meaning $\Delta G = \Delta A - k_B T$. Which in turn yields $\Delta G_{\mathrm{ads}} = -53 \pm 6$ meV from the simulations in this thesis and can be compared to the TI reference article that reports $\Delta G_{\mathrm{ads,ref.}} = -58 \pm 5$ meV [1]. As seen, both the final result and the individual terms presented in the tables 4.2 and 4.3 agree well.

The anharmonic and harmonic free energy can be compared to analyze the validity

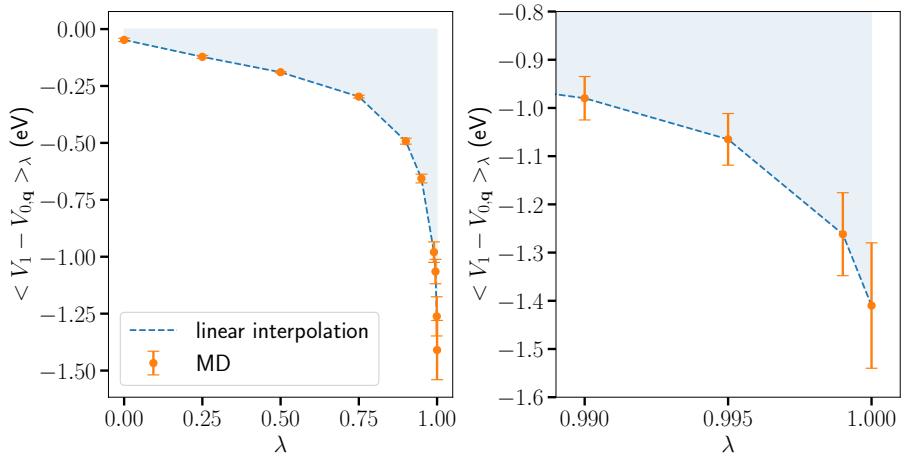

Figure 4.17: Averages $\langle V_1 - V_{0,\boldsymbol{q}} \rangle_\lambda$ to compute the harmonic to DFT correction term $\Delta A_{0,\boldsymbol{q} \longrightarrow 1}$ for N_2 in H-CHA.

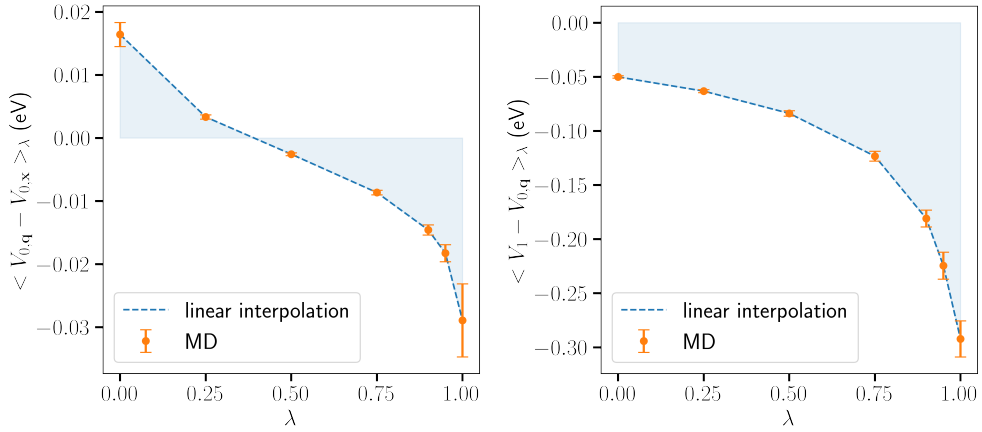

Figure 4.18: Averages to compute the correction terms for the empty H-CHA. (left) $\Delta A_{0,\boldsymbol{x} \longrightarrow 0,\boldsymbol{q}}$, (right) $\Delta A_{0,\boldsymbol{q} \longrightarrow 1}$.

of the approximation. For the clean H-CHA the free energy using the unmodified eigenvalues gives $A_{\mathrm{H-CHA,harm.}} = -287.071$ eV and the modified spectrum and anharmonic correction terms $A_{\mathrm{H-CHA,anharm.}} = -287.072$ eV. The difference is negligible (less than 0.001 eV) and shows that the harmonic approximation is acceptable for the clean H-CHA. However, for N_2@H-CHA $A_{\mathrm{N_2@H-CHA,harm.}} = -303.975$ eV and $A_{\mathrm{N_2@H-CHA,anharm.}} = -303.997$ eV, showing that the anharmonic correction lowers the free energy by 0.021 eV, in other words describes the system as more stable. The TI reference article reports the corresponding decrease of free energy by 0.029 eV [1].

Table 4.1: Terms contributing to A_0 at 200 K and 101.325 kPa. For the two zeolite systems, $A_{\text{vib,mod.}}$ is with the modified Hessian, in other words where the smallest eigenvalues has been increased.

system	A_{el}	$A_{\text{vib,unmod.}}$	$A_{\text{vib,mod.}}$	$A_{\text{trans,rot}}$	switch to G
N_2	-16.609	0.049	-	$-0.373 + \frac{5}{2}k_BT$	$k_BT = 0.017$
H-CHA	-289.120	2.050	2.153	-	pV
N_2@H-CHA	-306.052	2.077	2.318	-	pV

Table 4.2: Free energy contributions to A_1 in eV and at atmospheric pressure 101.325 kPa. (a): This value represents $G_0 = A_{0,\boldsymbol{x}} - k_BT$, where $A_{0,\boldsymbol{x}}$ includes electronic energy A_{el}, and classical harmonic approximation for vibrations $A_{\text{vib,unmod.}}$, ideal gas, free translator and rigid rotor approximations.

system	$A_{0,\boldsymbol{x}}$	$\Delta A_{0,\boldsymbol{x}\longrightarrow 0,\boldsymbol{q}}$	$\Delta A_{0,\boldsymbol{q}\longrightarrow 1}$	A_1
N_2	$16.933^{(a)}$	0	0	$-16.873^{(a)}$
H-CHA	-286.967	-0.003 ± 0.000	-0.102 ± 0.002	-287.072 ± 0.002
N_2@H-CHA	-303.734	-0.018 ± 0.001	-0.244 ± 0.003	-303.997 ± 0.004

Table 4.3: Shows the same terms as table 4.2 but the values are copied from the TI reference article [1, Table 2]. Contributions to the Free Energies A_1 in eV at 200 K at a pressure of 101.325 kPa. The description of the values is slightly modified to be more consistent with the notation used in the thesis. (a): This value represents $G_0 = A_{0,\boldsymbol{x}} - k_BT$, where $A_{0,\boldsymbol{x}}$ includes electronic energy A_{el}, classical harmonic approximation for vibrations A_{vib}, ideal gas, free translator and rigid rotor approximations.

system	$A_{0,\boldsymbol{x}}$	$\Delta A_{0,\boldsymbol{x}\longrightarrow 0,\boldsymbol{q}}$	$\Delta A_{0,\boldsymbol{q}\longrightarrow 1}$	A_1
N_2	$-16.873^{(a)}$	0	0	$-16.873^{(a)}$
H-CHA	-286.968	-0.005 ± 0.000	-0.099 ± 0.001	-287.072 ± 0.004
N_2@H-CHA	-303.736	-0.022 ± 0.001	-0.245 ± 0.005	-304.003 ± 0.005

4.2.3 $[Cu(NH_3)_2]^+$ adsorbed in CHA

Just as for N_2@H-CHA the dynamics of the system driven by $V_{0,\boldsymbol{x}}$, $V_{0,\boldsymbol{q}}$ or V_1 can be analyzed with some RDF. In this case, an RDF of the two N with the reference atom Al in the zeolite is seen in fig. 4.19 and in fig. 4.20 the RDF of Cu with the same reference atom Al. No periodic conditions are used so it is always the Al that belongs to the zeolite cage the $[Cu(NH_3)_2]^+$ is inside, and $[Cu(NH_3)_2]^+$ never leaves the initial zeolite cage. The RDF shows similar characteristics as N_2@H-CHA with the harmonic potential $V_{0,\boldsymbol{x}}$, barely leaving its initial position for both N and Cu. In fig. 4.19 the RDF is 0 between the peaks, indicating that no rotation has occurred. This clearly visualizes how constrained the dynamics are with the harmonic approximation in $\boldsymbol{x}$.

Further, with $V_{0,\boldsymbol{q}}$ there are noticeable differences compared to N_2@H-CHA , namely that the corresponding RDF is almost identical to the one for $V_{0,\boldsymbol{x}}$. The peak of $\mathrm{RDF}_{\mathrm{Cu-Al}}$ with $V_{0,\boldsymbol{q}}$ is slightly wider than with $V_{0,\boldsymbol{x}}$, otherwise very similar. $[Cu(NH_3)_2]^+$ is clearly also constrained with the harmonic approximation in $\boldsymbol{q}$. This poses the question of whether the internal coordinates were chosen properly, however when observing the averages $\langle V_{0,\boldsymbol{q}} - V_{0,\boldsymbol{x}} \rangle_\lambda$ in fig. 4.22 and the subsequent correction term $\Delta A_{0,\boldsymbol{x}\longrightarrow 0,\boldsymbol{q}} = \int_{\lambda=0}^{1} \langle V_{0,\boldsymbol{q}} - V_{0,\boldsymbol{x}} \rangle_\lambda \, \partial\lambda$, presented in table 4.5, it is obvious much is happening beyond what the RDF shows. Considering fig. 4.22 the average is practically zero until reaching $\lambda > 0.99$ when the average energy difference begins to increase drastically and is a quite good demonstration of the procedure of TI and how essential the internal coordinates are for this type of application of TI. Firstly, even when the intermediate potential V_λ only has a small contribution from $V_{0,\boldsymbol{x}}$, the harmonic potentials are so steep that they still limit the moveability of $[Cu(NH_3)_2]^+$. However, when the MD is completely, or almost completely, driven by $V_{0,\boldsymbol{q}}$ (close to $\lambda = 1$), the atoms move far enough from their modes minima that the energy calculated with $V_{0,\boldsymbol{x}}$ is extremely large. Secondly, without the use of internal coordinates the averages $\langle V_1 - V_{0,\boldsymbol{x}} \rangle_\lambda$ would be required to be calculated directly. One can see that with V_1, $\mathrm{RDF}_{\mathrm{N-Al}}$ and $\mathrm{RDF}_{\mathrm{Cu-Al}}$ is smeared out, showing the increased translational and rotational freedom. With the apparently limited extra movement $V_{0,\boldsymbol{q}}$ introduced, as evident in the RDFs in figs. 4.19 and 4.20, and the still large energy differences shown in fig. 4.22, a direct transition from $V_{0,\boldsymbol{x}}$ to V_1 would be likely come with so large energy differences, together with expensive DFT calculations, that convergence would never be reached within a reasonable amount of time.

An interesting observation is that the showed RDFs for $[Cu(NH_3)_2]^+$ driven by V_1 are much broader than for the smaller molecule N_2 shown earlier in fig. 4.15. Although the temperature for the simulation with $[Cu(NH_3)_2]^+$@CHA is 473 K and N_2@H-CHA is at 200 K, intuitively one could presume that the small N_2 would be able to be less constrained in H-CHA than $[Cu(NH_3)_2]^+$@CHA , as seen in the CPES simulations in figs. 4.6 and 4.7. However, there are other computational differences in the simulations, such as van der Waals correction. This topic is further discussed in 5.

All computed averages for $[Cu(NH_3)_2]^+$@CHA are seen in figs. 4.22, 4.21 and for the clean CHA the averages are seen in fig. 4.23. The simulations and averages for the clean CHA are quite uneventful, with no quick changes with increasing λ and the errors are small.

A summary of the terms contributing to $A_{0,\boldsymbol{x}}$ is seen in table 4.4 and the terms contributing to A_1 in table 4.5. With $A_{0,\boldsymbol{x}}$ with the modified eigenvalues for the zeoliten systems and G_0 for the gas phase $[Cu(NH_3)_2]^+$, the naive Gibbs free energy of adsorption is $\Delta G_{\text{ads}} = A_{1,[Cu(NH_3)_2]^+@CHA} - A_{1,CHA} - G_{0,[Cu(NH_3)_2]^+} = -5.151 \pm 0.022$ eV. This expression of the adsorption free energy is not physically sound, a more realistic reaction would be $\Delta G_{\text{ads}} = A_{1,[Cu(NH_3)_2]^+@CHA} - A_{1,Cu-CHA} - 2G_{0,NH_3}$ but that requires simulations and calculations of additional systems.

Just as for N_2@H-CHA , the appropriateness of using the harmonic approximation for the clean CHA and $[Cu(NH_3)_2]^+$@CHA is enlightening to investigate. With the modified eigenvalues and corresponding anharmonic correction terms from TI, the Helmholtz free energy for the clean CHA is $A_{1,CHA} = -283.835 \pm 0.007$ eV, while the free energy with only the harmonic approximation is $A_{0,\boldsymbol{x},CHA} = -283.840$ eV. In this context are they almost identical, only differing by 5 meV. However, the free energies using the modified and unmodified Hessian for $[Cu(NH_3)_2]^+$@CHA is $A_{1,\text{mod.}} = -326.841 \pm 0.015$ eV and $A_{0,\boldsymbol{x},\text{unmod.}} = -326.632$ eV, in this case the anharmonic corrections lower the free energy with 209 meV from the harmonic approximation. Indeed, a substantial anharmonicity is present in this system.

Table 4.4: Terms contributing to A_0 at 473 K and 101.325 kPa. For the two zeolite systems, $A_{\text{vib,mod.}}$ is with the modified Hessian, in other words where the smallest eigenvalues has been increased.

system	A_{el}	$A_{\text{vib,unmod.}}$	$A_{\text{vib,mod.}}$	$A_{\text{trans,rot}}$	switch to Gibbs ens.
$[Cu(NH_3)_2]^+$	-37.497	0.672		-1.071	$k_BT = 0.041$
CHA	-284.852	1.012	1.387		pV
$[Cu(NH_3)_2]^+$@CHA	-327.808	1.176	2.073		pV

Table 4.5: Free energy contributions to A_1 in eV and atmospheric pressure 101.325 kPa and 473 K. (a) This value is actually the Gibbs free energy $G_0 = A_{0,\boldsymbol{x}} + k_BT$, just as in table 4.2.

system	$A_{0,\boldsymbol{x}}$	$\Delta A_{0,\boldsymbol{x}\longrightarrow 0,\boldsymbol{q}}$	$\Delta A_{0,\boldsymbol{q}\longrightarrow 1}$	A_1
$[Cu(NH_3)_2]^+$	-37.896	0	0	-37.896
CHA	-283.464	-0.010 ± 0.000	-0.361 ± 0.006	-283.835 ± 0.007
$[Cu(NH_3)_2]^+$ @CHA	-325.736	-0.299 ± 0.006	-0.806 ± 0.009	-326.796 ± 0.015

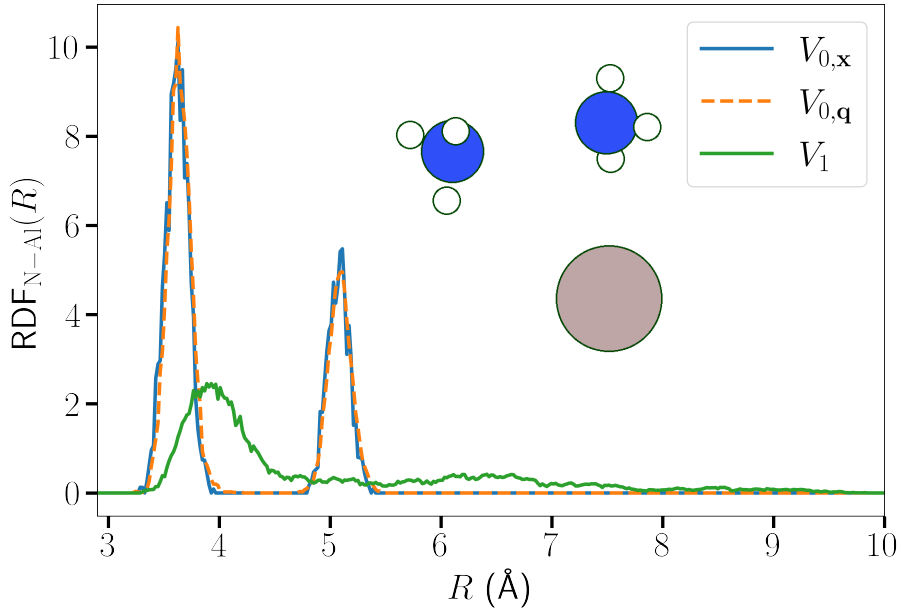

Figure 4.19: RDF of the distance between the N atoms and Al for $[Cu(NH_3)_2]^+$ in H-CHA. The distance is always the distance for atoms in the original unit cell, the $[Cu(NH_3)_2]^+$ stayed in the zeolite pore during the whole simulation.

4.2.3.1 Extracting entropy from anharmonic free energy

The anharmonic entropy from the TI method for N_2@H-CHA and $[Cu(NH_3)_2]^+$@CHA is found using the method described in section 2.6.5 for the two zeolite systems. The entropy and internal energy of gas phase N_2 were as before approximated as an ideal gas, free translator, rigid rotor and harmonic vibrations. The harmonic approximation for the adsorption entropy in the quantum mechanical description for the N_2@H-CHA system is $T\Delta S_{0,\mathrm{mod.}} = -0.385$ eV, using the modified eigenvalue spectrum. Then with $\alpha_{\mathrm{S},N_2@\mathrm{H-CHA}} = 0.61$ and $\alpha_{\mathrm{S,H-CHA}} = 0.62$, as defined in eq. (2.74), and $\Delta U_{\mathrm{ZPE},N_2@\mathrm{H-CHA}} = 0.109$ eV, $\Delta U_{\mathrm{ZPE,H-CHA}} = 0.039$ eV, as defined in eq. (2.73). Finally, from eq. (2.75), we have the anharmonic adsorption entropy $T\Delta S_1 = -0.332$ eV.

Similarily, for $[Cu(NH_3)_2]^+$@CHA we have $\alpha_{\mathrm{S},[Cu(NH_3)_2]^+@\mathrm{CHA}} = 0.65$ and $\alpha_{\mathrm{S,CHA}} = 0.65$, $\Delta U_{\mathrm{ZPE},[Cu(NH_3)_2]^+@\mathrm{CHA}} = 0.194$ eV, $\Delta U_{\mathrm{ZPE,CHA}} = 0.068$ eV, the harmonic adsorption entropy $T\Delta S_{0,\mathrm{mod.}} = -0.891$ eV and finally the anharmonic adsorption entropy $T\Delta S_1 = -0.497$ eV.

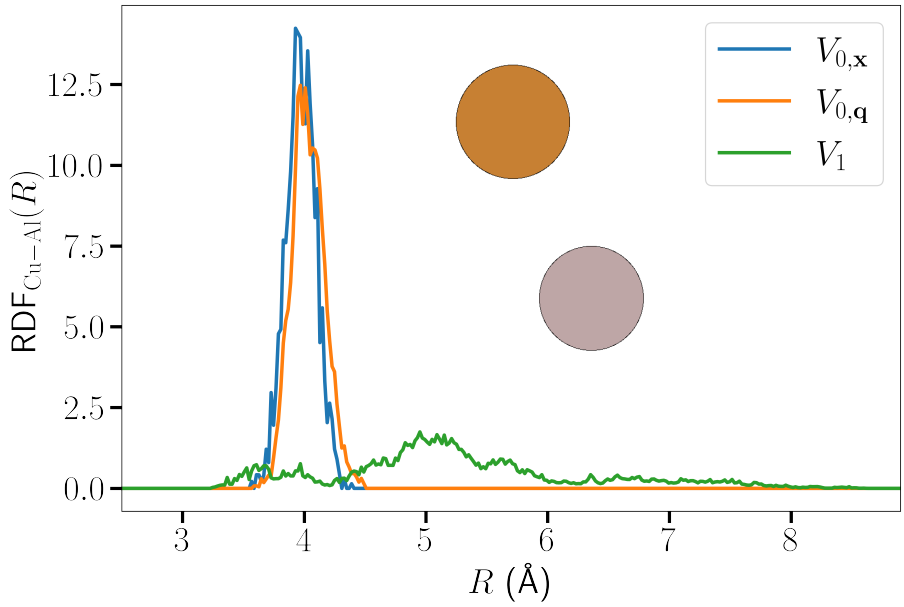

Figure 4.20: RDF of the distance between Cu and Al for $[Cu(NH_3)_2]^+$ in H-CHA. The distance is always the distance for atoms in the original unit cell, the $[Cu(NH_3)_2]^+$ stayed in the zeolite pore during the whole simulation.

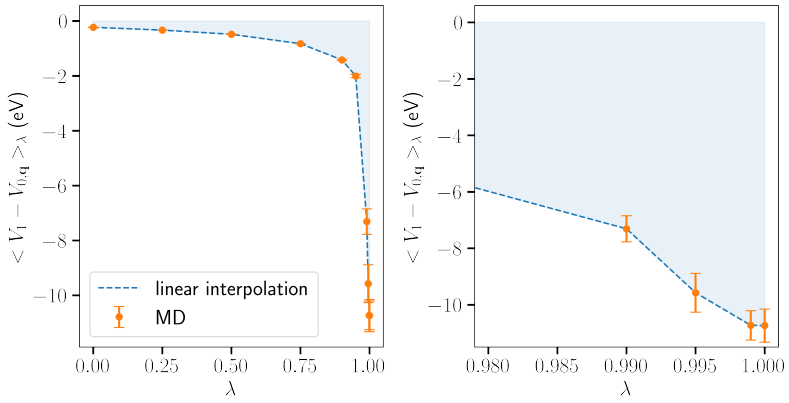

Figure 4.21: $A_{0,\boldsymbol{q}\longrightarrow 1}$ for $[Cu(NH_3)_2]^+$ in H-CHA.

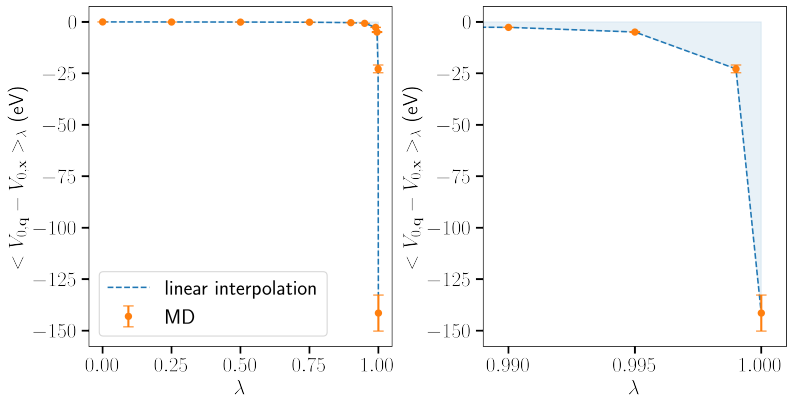

Figure 4.22: $A_{0,\boldsymbol{x}\longrightarrow 0,\boldsymbol{q}}$ for $[Cu(NH_3)_2]^+$ in H-CHA.

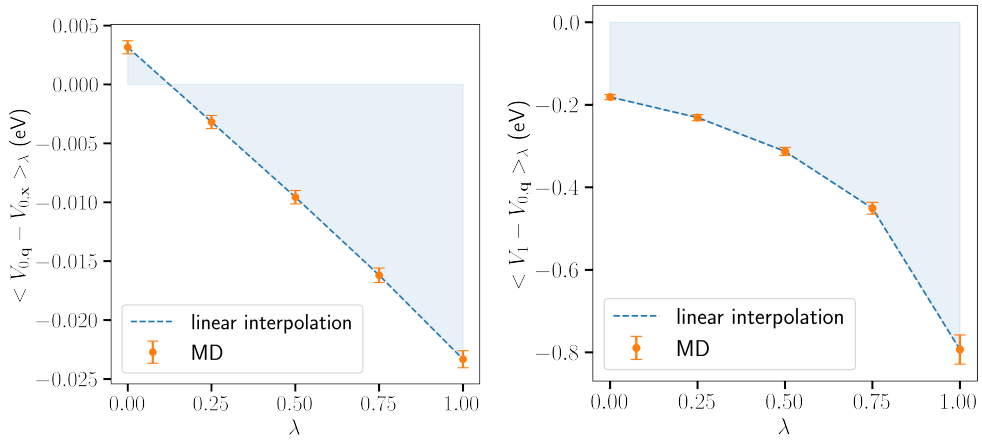

Figure 4.23: Averages to compute the correction terms for the empty CHA. (left) $\Delta A_{0,\boldsymbol{x}\longrightarrow 0,\boldsymbol{q}}$, (right) $\Delta A_{0,\boldsymbol{q}\longrightarrow 1}$.

4.2.4 Comparison of results

The reliability of the methods can in some sense be analyzed by comparing the results to experimental values and also comparing the results from the two studied methods. This is summarized in table 4.6. Preferably, the two methods would produce the same physical quantity. Unfortunately, this is not the case. The validity of the method to extract the entropy from the anharmonic free energy with TI is questionable and should not be seen as the main result of this thesis. Luckily, experimental data for both entropy and free energy exist for the N_2@H-CHA case. For $[Cu(NH_3)_2]^+$@CHA , merely a comparison between methods can be done, as well as overall observations comparing to N_2@H-CHA .

The experimental value of gas phase entropy N_2 at 200 K and standard pressure 101.325 kPa is 180 J/(mol K) [42] which corresponds to $TS_{N_2,\mathrm{NIST}} = 0.373$ eV. Compared to the theoretical value $S_{N_2} = 0.373$ eV using eqs. (2.26), (2.22), (2.24) is in good agreement. The vibrational contribution was in this case negligible.

At the same conditions the experimental adsorption entropy is $T\Delta S_{N_2@\mathrm{H-CHA,exp}} \approx -0.16$ eV and adsorption free energy $\Delta G_{N_2@\mathrm{H-CHA,exp}} = -0.045$ eV [5]. With the experimental adsorption entropy and gas phase entropy gives a $\gamma_{N_2@\mathrm{H-CHA,exp}} = 0.57$. The CPES adsorption entropy and γ agree fairly well with the experimental data, shown in table 4.6. From TI we have the primary result $\Delta G_{N_2@\mathrm{H-CHA,TI}} = -53 \pm 6$ meV, as mentioned in section 4.2.2, which was successfully reproduced from the reference article $G_{N_2@\mathrm{H-CHA,TI,ref.}} = -58 \pm 5$ meV [1]. Although the result is close to the experimental $\Delta G_{\mathrm{exp}} = -0.045$ eV, it overestimates how strong the adsorption is. This is shows more clearly when considering considering $\gamma_{N_2@\mathrm{H-CHA,TI}} = 0.11$, calculated using the secondary result from TI $T\Delta S_1 = -0.332$ eV.

For $[Cu(NH_3)_2]^+$@CHA at 473 K, the results were from CPES $T\Delta S_{[Cu(NH_3)_2]^+@\mathrm{CHA,trans,rot}} = -0.467$ eV, noting that the vibrational contribution is non-negligible as seen in table 4.4 and that γ should not include vibrational entropy, see eq. (2.46), giving a $\gamma_{[Cu(NH_3)_2]^+@\mathrm{CHA,CPES}} = 0.60$. From TI $\Delta G_{[Cu(NH_3)_2]^+@\mathrm{CHA,TI}} = -5.151$ eV is difficult to draw any conclusion since there is no value to compare it with. Also, as mentioned earlier, this adsorption from gas phase is unphysical as its calculated in this thesis. But, the secondary result $T\Delta S_{[Cu(NH_3)_2]^+@\mathrm{CHA,TI}}$ under the assumption that $[Cu(NH_3)_2]^+$ loses a negligible amount of vibrational entropy at adsorption, in other words all entropy decrease stems from limited translational and rotational freedom, and gives $\gamma = 0.58$. In this case, the γ values from CPES and TI are quite close, especially when compared to the large discrepancy in the N_2@H-CHA case. An important note here is that for N_2@H-CHA quite different simulation setups were used, while for $[Cu(NH_3)_2]^+$@CHA the simulation parameters were almost exactly the same.

The large difference in γ for N_2@H-CHA could be interpreted with the sampled coordinates for CPES in fig. 4.6 and the RDF from TI in fig. 4.15. Although there is a significant temperature difference and regular MD (not metadynamics) was used

Table 4.6: Summary of the results. Experimental values from [5, 42].

System and method	ΔG_{ads} (eV)	$T\Delta S_{\text{ads}}$ (eV)	γ
N_2@H-CHA (200 K)			
CPES		-0.130	0.65
TI	-0.053	-0.332	0.11
experimental	-0.045	-0.16	0.57
$[Cu(NH_3)_2]^+$@CHA (473 K)			
CPES		-0.467	0.60
TI	-5.151	-0.497	0.58

only in the first half of the CPES sampling, there is an obvious discrepancy in the dynamics of the adsorbed N_2 molecule. Therefore, an additional simulation using the exact parameters as in CPES but at 200 K for a production run of 8 ps and is compared to the corresponding RDF from the TI simulation, see fig. 4.24. The difference in the dynamics of the adsorbed N_2 is striking. With the CPES parameters, the wide RDF shows more similarity with the RDF of the large $[Cu(NH_3)_2]^+$, seen in fig. 4.19 and 4.20, than the RDF with two clear peaks from the simulation with TI parameters.

It could also be a coincidence that γ for $[Cu(NH_3)_2]^+$@CHA is similar and for N_2@H-CHA extremely different. However, the result shown in fig. 4.24 is in itself interesting since the same system is simulated but with different AIMD parameters and consequently, the behavior of the adsorbed N_2 is extremely different.

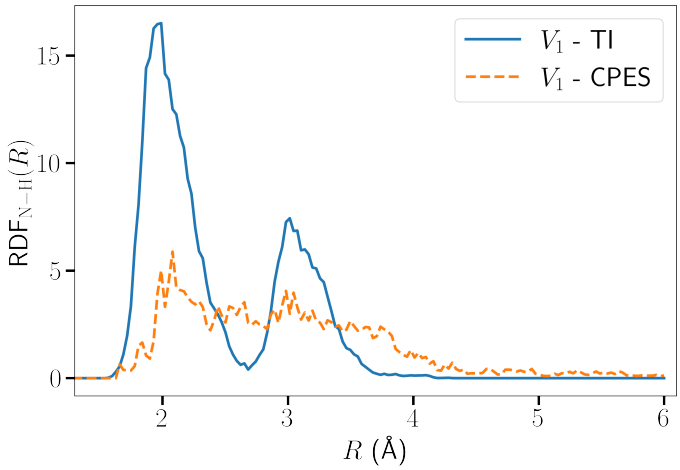

Figure 4.24: Comparison of RDF of N_2@H-CHA from the TI MD simulations with the DFT potential V_1 and a simulation of N_2@H-CHA with the parameters used in CPES but also at 200 K.

5
Discussion

In this chapter, the methods and results are discussed in general, and in detail about similarities and differences between the methods and possible reasons behind those. Also, drawbacks and suggestions for improvement are discussed.

5.1 CPES

5.1.1 Method and results

In this thesis, the CPES method applied to zeolite systems was attempted to be improved compared to previous implementations. Firstly, a dynamic zeolite framework was used to include diffusion and adsorption energy effects that might play a significant role in the construction of the PES, compared to previous implementations where the framework was fixed using either Monte Carlo sampling [32] or MTD [12]. As we saw in fig. 4.4 the non-fix zeolite framework seems to have some effect on the dynamics. Using the dynamic framework was done successfully by separating the adsorbed molecule and the zeolite for each MD step and calculating their static energy explicitly, giving a PES where the vibrations of both the adsorbed molecule and the zeolite structure were mostly eliminated, as was shown in fig. 4.3. A disadvantage of the new implementation is that it is more computationally demanding. To what extent the dynamic framework affects the PES could be evaluated more thoroughly.

Secondly, the change of CVs in the MTD to cartesian coordinates (x, y, z) of the center of mass of the adsorbed molecule, instead of distances and angles to atoms in the zeolite as used in previous work [12], was primarily necessary due to the dynamic framework in this thesis, since the reference points (zeolite atoms) vibrate and showed to be a poor choice for N_2@CHA$-SiO_2$. The positive side effects of this are reduced complexity and a more simple choice of CVs. The MTD is only used to enhance the sampling of the PES by speeding up finding local energy minima by letting the adsorbed molecule explore the PES more naturally with MD, compared to static sampling of either the whole cell or using Monte Carlo. Since the added gaussians that construct a FES are not used, it is not necessarily bad with complex CVs. A combination of cartesian coordinates, and some angle between atoms in the molecule and the zeolite that describes the rotation of the adsorbed molecule, could further enhance the sampling. This would require that one or a few atoms in the zeolite is kept fixed and is believed to have a negligible effect on the PES.

Furthermore, one or a few fixed atoms would probably solve another issue, that the whole zeolite cage translates a few Å when the adsorbed molecule diffused to another cell, which is a critical problem since the whole PES coordinate system is as a consequence shifted. Those samples had to be discarded in this thesis and the possibility to sample near the zeolite rings was limited. Some fixed atoms in the zeolite would probably prevent the translation of the whole cell and the adsorbate that diffused into another cell could simply be folded back inside the original cell in the post-processing of the data. The parameters τ_G, w, h for the CVs could be tuned more extensively, but due to the slow nature of trial and error with DFT driven MTD and the time constraint of the thesis, this was not possible. As seen in the figs. 4.5 4.6 and 4.7 however, MTD quite clearly assists the exploration and thus sampling, hence the parameter selection was deemed adequate.

Thirdly, the integration of the PES was done differently in this thesis compared to previous implementations where a summation was used [32, 12]. Using Simpson's rule, or even the trapezoidal rule, should give more accurate integration.

The implementation of the method seems correct since the result for N_2@CHA$-SiO_2$ is close to previous values reported in [12], when corrected for pressure, as well as the entropy for N_2@CHA$-SiO_2$ in fig. 4.11 can be compared with [32, Figure 4], where we see that TS for N_2@CHA$-SiO_2$ are in excellent agreement. Contrary to the points mentioned above, the attempts to improve the CPES method might have only negligible impact, since the results are similar to the previous.

For N_2@H-CHA the entropy is also in quite good agreement with experimental values, which further gives confidence in the implementation of the method and thus for the $[Cu(NH_3)_2]^+$ case. Although the assumption that $[Cu(NH_3)_2]^+$ is linear could perhaps be too naive since the angle between the N atoms varies extensively in the MD. This missing contribution could perhaps be accounted for by including the corresponding vibrational mode to the vibrational entropy, as this vibration should not have too large hindering nor facilitating influence on the translation and rotation. Even though it was noted above that the attempted improvements of CPES might not be significant for N_2, the method the eliminate the vibrations is probably more important for $[Cu(NH_3)_2]^+$, with the reasoning that the vibrations are more prominent, as is seen in fig. 4.2 where the framework is fixed and it is difficult to distinguish the $[Cu(NH_3)_2]^+$ vibrations from the interactions with the zeolite. Another solution to possibly eliminate the vibrations would be to find the vibrational modes of the adsorbed molecule and filter out the frequencies from the energy of the MD trajectory, but then the interaction with the dynamic zeolite is neglected. The interaction of $[Cu(NH_3)_2]^+$ and the dynamic framework might have a larger influence than for N_2 , as the $[Cu(NH_3)_2]^+$ is more stuck and therefore have stronger interaction with the zeolite.

5.1.2 Further improvements

An improvement to the CPES method, as a whole, would be to use the partition function Z_{CPES} to also compute the translational and rotational internal energy and/or the free energy directly, using eq. (2.29) or eq. (2.15), respectively. Then with CPES, the full anharmonic free energy contribution from translation and rotation of the adsorbed molecule can be calculated. The anharmonic free energy from CPES could then be compared directly with the free energy from TI, where CPES has the advantage of that the entropy and internal energy, or enthalpy, are separated and could therefore be analyzed individually and possibly also corrected to experimental data. However, a major disadvantage of finding the internal energy with CPES is that the method is sensitive to energy and configurational fluctuations since the internal energy is not independent of an arbitrary energy shift of the PES. Thus, instantaneous structures where the energy $U(\mathbf{r}, \phi)$ is lower than that of the relaxed system might largely influence the internal energy. An example would be if one H atom in the $[Cu(NH_3)_2]^+$@CHA system shortly binds to the Al instead of N, which is another system than the studied and could differ largely in $U(\mathbf{r}, \phi)$. These situations obviously would impact the entropy as well, but probably not to the same extent due to the entropy's invariance to an arbitrary shift. Therefore, it is suggested to discard structures that do not correspond to the actual studied system, by for example using maximum bond lengths criteria and investigating the MD trajectory where $U(\mathbf{r}, \phi)$ is unusually low. Then, the lowest energy of the PES should be near that of the relaxed system, so that the lowest PES energy $U(\mathbf{r}, \phi)$ can be shifted to 0 and therefore will CPES only include translational and rotational contributions from the sampled PES. These energy fluctuations do not pose a problem in the TI method since they become non-influential to the energy average due to the long MD trajectories.

Generally, the sampling of the PES and exploration of local minima can always be improved for complex multidimensional systems such as those studied in this thesis. However, a more obvious improvement lies in the computation of the integral in eq. (2.44). As mentioned in section 3.3.3, the whole interpolated grid is stored in the memory, which vastly limits the grid resolution due to memory constraints. This is unnecessary because the integral can easily be split up into multiple integrals that can be stored in memory and calculated separately, thus allowing for a larger grid resolution. For example, the center of mass space could be divided into smaller volumes, or use smaller (volume) sections where the sampling is denser. Then one could investigate the impact the integration method actually has on the final entropy, comparing the summation used in [32, 12] to Simpson's rule with various grid resolutions. Further validation of the implemented method in this thesis could more extensively be performed, investigating convergence with respect to grid resolution, number of data points, etc.

It would also be interesting to consider interpolating the PES using Gaussian Processes (GPs) instead of linear interpolation, which could lead to fewer samples and a quantitative measure of the uncertainty [11]. In the current implementation of CPES, the error is not estimated, and with GPs this could be possible. Even if the

current implementation with linear interpolation is used, the development of some sort of error estimate would be beneficial, and here lies a disadvantage compared to TI where the error is estimated.

5.2 TI

5.2.1 Method and results

The results of the HF molecule and N_2@H-CHA were successfully reproduced from the TI reference article [1]. An interesting result, as they also concluded, is that vibrations even for a large system as a zeolite are well approximated with the harmonic approximation, whereas for a zeolite system the difference between harmonic and anharmonic free energy was only about 5 meV.

The RDF figures are a great tool to analyze both what the different potentials introduce regarding dynamics, as well as how different simulation setups large influence the adsorbate dynamics. By the more smooth RDF for V_1 potentials compared to harmonic, it is clear how the harmonic approximation is a too strict description of weakly adsorbed molecules. This also further demonstrates the necessity of using the internal coordinates as an intermediate coordinate system when transforming from the harmonic in cartesian coordinates to DFT, where the RDF peaks only slightly change for $V_{0,\boldsymbol{q}}$ compared to $V_{0,\boldsymbol{x}}$, meaning that $V_{0,\boldsymbol{x}}$ is very sensitive to atoms translating not even far from the minima of the (cartesian) harmonic potentials since the correction term $\Delta A_{0,\boldsymbol{x}\longrightarrow 0,\boldsymbol{q}}$ is non-negligible and of the same order of magnitude as $\Delta A_{0,\boldsymbol{q}\longrightarrow 1}$. The strictness of $V_{0,\boldsymbol{x}}$ can also be observed in the $\langle V_{0,\boldsymbol{q}} - V_{0,\boldsymbol{x}}\rangle_\lambda$ figs. 4.16 and 4.22 for N_2@H-CHA and $[Cu(NH_3)_2]^+$@CHA , respectively. For $\lambda = 0$ up to $\lambda = 0.990$ the average is essentially 0, meaning that even if the system is driven to 99% by $V_{0,\boldsymbol{q}}$ its low energy configurations are never reached since $V_{0,\boldsymbol{x}}$ is narrow. Although, at higher λ, up to $\lambda = 1$, the impact of $V_{0,\boldsymbol{q}}$ is noticable as $V_{0,\boldsymbol{x}}$ increase to very large values. An interesting observation is that even with long simulations for $\langle V_{0,\boldsymbol{q}} - V_{0,\boldsymbol{x}}\rangle_{\lambda=1}$, the standard error is many times larger than of the corresponding average $\langle V_1 - V_{0,\boldsymbol{q}}\rangle_{\lambda=1}$. Due to that $\Delta A_{0,\boldsymbol{x}\longrightarrow 0,\boldsymbol{q}}$ is much more computationally inexpensive compared to $\Delta A_{0,\boldsymbol{q}\longrightarrow 1}$, it would probably be preferred to include as much translational and rotational freedom as possible in the internal coordinates $\boldsymbol{q}$.

5.2.2 Further improvements

The choice of internal coordinates of $[Cu(NH_3)_2]^+$ would perhaps be improved for the coordinate describing the relation between the two NH_3. In the current implementation, the distance between the two N atoms is used to constrain the angle between them, otherwise, the molecule would collapse. An angle coordinate instead would perhaps allow for larger deviations from a completely linear molecule and therefore be more similar to the dynamics during AIMD. This could possibly be solved by shifting the angle by 180° to avoid the numerical problems near a straight

angle due to the discontinuity.

If more and even longer simulations with the hMD program are required to reach smaller standard errors, some performance optimization or parallelization might be a good improvement.

5.3 Overall comparison

Regarding TI, whether the introduced method to extract entropy from the free energy and consequently calculate γ, is unreliable, we clearly see that the simulation setup strongly influences the dynamics of the adsorbate and therefore also the free energy. This was seen both when comparing the RDF for N_2@H-CHA (fig. 4.15) with $[Cu(NH_3)_2]^+$@CHA (figs. 4.19 and 4.20, as well as with the additional MD for N_2@H-CHA with simulation parameters used in CPES, except at 200 K instead, shown in fig. 4.24. The large $[Cu(NH_3)_2]^+$ moves substantially more than N_2 , however at a higher temperature. Thus, the additional MD is perhaps a more fair comparison, where the difference still is very obvious. With the TI parameters N_2 is essentially stuck compared with the MD with CPES parameters. Major differences in the simulation setup are the van der Waals correction and thermostat, and as mentioned in the result chapter, the difference in dynamics is an interesting result in itself. So, the simulation setup seems to be crucial and it would be interesting to continue a more thorough investigation into what lies behind the difference. The Andersen thermostat seems to give similar results as Nosé-Hoover for $[Cu(NH_3)_2]^+$@CHA, but not for N_2@H-CHA, perhaps is the temperature of 200 K not suitable for the combination of the system N_2@H-CHA and Andersen thermostat, i.e. describing the phase space poorly in this case. There is probably not an issue with an unequilibrated system since both reproduced RDF and results are in good agreement with the TI reference [1, Figure 6]. Or, could it be the importance of accurate van der Waals interactions for weakly adsorbed molecules?

As CPES has the advantage of describing the entropy for a wide temperature range, while TI only computes the free energy (and entropy) for a single temperature at a time, but perhaps more accurately. A possibility to utilize both methods is to validate the CPES calculations with one or more TI calculations at different temperatures. Even some calibration schemes could be a possibility. When more systems are studied the found entropies/free energies can be used in simulated temperature programmed desorption (TPD) [13] and compare to experimental TPD.

The long simulations using TI might be mitigated using machine learning (ML) force fields instead of DFT, implemented in VASP 6.3 [29]. This would require a well-trained ML model for the system, which might be difficult to achieve. It would perhaps also require training on structures gained when the system is driven by harmonic potentials, as these configurations else would give large errors. A good model could also be reused for CPES, and the whole coordinate space would probably be possible to sample. Or, use it in combination with GPs and explore based on the GP model's uncertainty.

6
Conclusion

The aim of the thesis was to accurately calculate the anharmonic entropies of weakly adsorbed molecules, specifically N_2@CHA$-SiO_2$, N_2@H-CHA and $[Cu(NH_3)_2]^+$@CHA. To do this two methods were investigated, namely Complete Potential Energy Sampling in combination with metadynamics and Thermodynamic Integration using intermediate internal coordinates. The correct implementation of the methods was validated by reproducing results from previous studies. At 200 K for N_2@H-CHA , the reference experimental adsorption entropy was $T\Delta S_{\text{exp}} = -0.16$ eV, while with CPES $T\Delta S_{\text{CPES}} = -0.13$ eV and with TI $T\Delta S_{\text{TI}} = -0.33$ eV. Or, on the form where the adsorbate translational and rotational entropy is the fraction γ of the gas phase translational and rotational entropy, $\gamma_{\text{exp}} = 0.57$, $\gamma_{\text{CPES}} = 0.65$ and $\gamma_{\text{TI}} = 0.11$. At 473 K for $[Cu(NH_3)_2]^+$@CHA the adsorption entropy (from gas phase) was with CPES $T\Delta S_{\text{CPES}} = -0.467$ eV and with TI $T\Delta S_{\text{TI}} = -0.497$ eV, and correspondingly $\gamma_{\text{CPES}} = 0.60$ and $\gamma_{\text{TI}} = 0.58$. The discrepancy between CPES and TI for N_2 was discussed, and the possible reasons could be the perhaps unreliable procedure to extract entropy from free energy, thermostat, and the van der Waals correction. Furthermore, it was concluded from the findings with TI that the harmonic approximation is valid for systems with only vibrational degrees of freedom, i.e. even for relatively large systems such as (clean) zeolites the anharmonicity is negligible.

In the thesis, an improvement to CPES with metadynamics was introduced, that eliminated vibrations from the translation and rotational PES, as well as accounting for dynamic interactions with the zeolite, by recalculating the electronic energy of the instantaneous and separated adsorbate and zeolite structures. It was also suggested to use CPES, with the same PES, to also calculate anharmonic contributions to the enthalpy. An advantage of CPES is that the entropy is found for a range of temperatures based on the same PES. Also, CPES is complemented well with MD/MTD, since local minima configurations of the PES are more likely to be visited during simulations and they contribute the most to the entropy. The advantages of TI are better quantification of convergence and errors, lower sensitivity to unphysical energy fluctuations, and with increasingly complex adsorbates, it is probably easier to describe the configurations with internal coordinates than with a potential energy surface, as in CPES. This thesis contributes to the field by successful reproduction of others' results, and further compares, evaluates and suggests improvements to CPES and TI, and calculates entropy for a new system, $[Cu(NH_3)_2]^+$@CHA.

Bibliography

[1] Jonas Amsler, Philipp N. Plessow, Felix Studt, and Tomáš Bučko. Anharmonic correction to adsorption free energy from dft-based md using thermodynamic integration. *Journal of Chemical Theory and Computation*, 17(2):1155–1169, 2021. PMID: 33482059.

[2] Hans C. Andersen. Molecular dynamics simulations at constant pressure and/or temperature. *The Journal of Chemical Physics*, 72(4):2384–2393, 1980.

[3] Vladimir I. Anisimov, Jan Zaanen, and Ole K. Andersen. Band theory and mott insulators: Hubbard u instead of stoner i. *Phys. Rev. B*, 44:943–954, Jul 1991.

[4] C. Bradford Barber, David P. Dobkin, and Hannu Huhdanpaa. The quickhull algorithm for convex hulls. *ACM Trans. Math. Softw.*, 22(4):469–483, dec 1996.

[5] R. M. Barrer and J. A. Davies. Sorption in decationated zeolites. i. gases in hydrogen-chabazite. *Proceedings of the Royal Society of London. Series A, Mathematical and Physical Sciences*, 320(1542):289–308, 1970.

[6] P. E. Blöchl. Projector augmented-wave method. *Phys. Rev. B*, 50:17953–17979, Dec 1994.

[7] G. Bussi and A. Laio. Using metadynamics to explore complex free-energy landscapes. *Nat Rev Phys*, 2:200–212, 2020.

[8] Sebastián Caro-Ortiz, Erik Zuidema, Marcello Rigutto, David Dubbeldam, and Thijs J. H. Vlugt. Effects of framework flexibility on the adsorption and diffusion of aromatics in mfi-type zeolites. *The Journal of Physical Chemistry C*, 124(44):24488–24499, 2020.

[9] Lin Chen. Surface phase diagrams from first principles, May 2022.

[10] C.J. Cramer. *Essentials of Computational Chemistry: Theories and Models*. John Wiley and Sons Ltd, second edition edition, 2004.

[11] Volker L. Deringer, Albert P. Bartók, Noam Bernstein, David M. Wilkins, Michele Ceriotti, and Gábor Csányi. Gaussian process regression for materials and molecules. *Chemical Reviews*, 121(16):10073–10141, 2021. PMID: 34398616.

[12] Philip Edenborg. First principles calculations of molecular entropies in zeolites, the effect of different counter ions. Master's thesis, Chalmers University of Technology, 2019.

[13] Yingxin Feng. *Reaction kinetics of NH_3−SCR over Cu-CHA from first principles*. Licentiate thesis, Chalmers University of Technology, Gothenburg, Sweden, 2021.

[14] Yingxin Feng, Ton V. W. Janssens, Peter N. R. Vennestrøm, Jonas Jansson, Magnus Skoglundh, and Henrik Grönbeck. The role of h+- and cu+-sites for

n2o formation during nh3-scr over cu-cha. *The Journal of Physical Chemistry C*, 125(8):4595–4601, 2021.

[15] Yingxin Feng, Xueting Wang, Ton V. W. Janssens, Peter N. R. Vennestrøm, Jonas Jansson, Magnus Skoglundh, and Henrik Grönbeck. First-principles microkinetic model for low-temperature nh3-assisted selective catalytic reduction of no over cu-cha. *ACS Catalysis*, 11(23):14395–14407, 2021.

[16] H. Flyvbjerg and H. G. Petersen. Error estimates on averages of correlated data. *The Journal of Chemical Physics*, 91(1):461–466, 1989.

[17] Daniel Foreman-Mackey. corner.py: Scatterplot matrices in python. *The Journal of Open Source Software*, 1(2):24, jun 2016.

[18] Daan Frenkel and Berend Smit. Chapter 4 - molecular dynamics simulations. In Daan Frenkel and Berend Smit, editors, *Understanding Molecular Simulation (Second Edition)*, pages 63–107. Academic Press, San Diego, second edition edition, 2002.

[19] Daan Frenkel and Berend Smit. Chapter 6 - molecular dynamics in various ensembles. In Daan Frenkel and Berend Smit, editors, *Understanding Molecular Simulation (Second Edition)*, pages 139–163. Academic Press, San Diego, second edition edition, 2002.

[20] Daan Frenkel and Berend Smit. Chapter 7 - free energy calculations. In Daan Frenkel and Berend Smit, editors, *Understanding Molecular Simulation (Second Edition)*, pages 167–200. Academic Press, San Diego, second edition edition, 2002.

[21] Daria Ruth Galimberti and Joachim Sauer. Chemically accurate vibrational free energies of adsorption from density functional theory molecular dynamics: Alkanes in zeolites. *Journal of Chemical Theory and Computation*, 17(9):5849–5862, 2021. PMID: 34459582.

[22] Stefan Grimme. Semiempirical gga-type density functional constructed with a long-range dispersion correction. *Journal of Computational Chemistry*, 27(15):1787–1799, 2006.

[23] Stefan Grimme, Jens Antony, Stephan Ehrlich, and Helge Krieg. A consistent and accurate ab initio parametrization of density functional dispersion correction (dft-d) for the 94 elements h-pu. *The Journal of Chemical Physics*, 132(15):154104, 2010.

[24] Charles R. Harris, K. Jarrod Millman, Stéfan J. van der Walt, Ralf Gommers, Pauli Virtanen, David Cournapeau, Eric Wieser, Julian Taylor, Sebastian Berg, Nathaniel J. Smith, Robert Kern, Matti Picus, Stephan Hoyer, Marten H. van Kerkwijk, Matthew Brett, Allan Haldane, Jaime Fernández del Río, Mark Wiebe, Pearu Peterson, Pierre Gérard-Marchant, Kevin Sheppard, Tyler Reddy, Warren Weckesser, Hameer Abbasi, Christoph Gohlke, and Travis E. Oliphant. Array programming with NumPy. *Nature*, 585(7825):357–362, September 2020.

[25] P. Hohenberg and W. Kohn. Inhomogeneous electron gas. *Phys. Rev.*, 136:B864–B871, Nov 1964.

[26] William G. Hoover. Canonical dynamics: Equilibrium phase-space distributions. *Phys. Rev. A*, 31:1695–1697, Mar 1985.

[27] William G. Hoover. Constant-pressure equations of motion. *Phys. Rev. A*, 34:2499–2500, Sep 1986.

[28] J. D. Hunter. Matplotlib: A 2d graphics environment. *Computing in Science & Engineering*, 9(3):90–95, 2007.

[29] The Vienna Ab initio Simulation Package. Category:machine-learned force fields, 2022. Last accessed 5 June 2022.

[30] The Vienna Ab initio Simulation Package. Metadynamics, 2022. Last accessed 5 June 2022.

[31] Mikkel Jørgensen. *Kinetics of Nanoparticle Catalysis from First Principles*. Phd thesis, Chalmers University of Technology, Gothenburg, Sweden, 2019.

[32] Mikkel Jørgensen, Lin Chen, and Henrik Grönbeck. Monte carlo potential energy sampling for molecular entropy in zeolites. *The Journal of Physical Chemistry C*, 122(35):20351–20357, 2018.

[33] Mikkel Jørgensen and Henrik Grönbeck. Adsorbate entropies with complete potential energy sampling in microkinetic modeling. *The Journal of Physical Chemistry C*, 121(13):7199–7207, 2017.

[34] W. Kohn and L. J. Sham. Self-consistent equations including exchange and correlation effects. *Phys. Rev.*, 140:A1133–A1138, Nov 1965.

[35] G. Kresse and J. Furthmüller. Efficient iterative schemes for ab initio total-energy calculations using a plane-wave basis set. *Phys. Rev. B*, 54:11169–11186, Oct 1996.

[36] G. Kresse and J. Furthmüller. Efficiency of ab-initio total energy calculations for metals and semiconductors using a plane-wave basis set. *Computational Materials Science*, 6(1):15–50, 1996.

[37] G. Kresse and J. Hafner. Ab initio molecular dynamics for liquid metals. *Phys. Rev. B*, 47:558–561, Jan 1993.

[38] G. Kresse and D. Joubert. From ultrasoft pseudopotentials to the projector augmented-wave method. *Phys. Rev. B*, 59:1758–1775, Jan 1999.

[39] Alessandro Laio and Michele Parrinello. Escaping free-energy minima. *Proceedings of the National Academy of Sciences*, 99(20):12562–12566, 2002.

[40] Ask Hjorth Larsen, Jens Jørgen Mortensen, Jakob Blomqvist, Ivano E Castelli, Rune Christensen, Marcin Dułak, Jesper Friis, Michael N Groves, Bjørk Hammer, Cory Hargus, Eric D Hermes, Paul C Jennings, Peter Bjerre Jensen, James Kermode, John R Kitchin, Esben Leonhard Kolsbjerg, Joseph Kubal, Kristen Kaasbjerg, Steen Lysgaard, Jón Bergmann Maronsson, Tristan Maxson, Thomas Olsen, Lars Pastewka, Andrew Peterson, Carsten Rostgaard, Jakob Schiøtz, Ole Schütt, Mikkel Strange, Kristian S Thygesen, Tejs Vegge, Lasse Vilhelmsen, Michael Walter, Zhenhua Zeng, and Karsten W Jacobsen. The atomic simulation environment—a python library for working with atoms. *Journal of Physics: Condensed Matter*, 29(27):273002, 2017.

[41] Samuel L. C. Moors, Kristof De Wispelaere, Jeroen Van der Mynsbrugge, Michel Waroquier, and Veronique Van Speybroeck. Molecular dynamics kinetic study on the zeolite-catalyzed benzene methylation in zsm-5. *ACS Catalysis*, 3(11):2556–2567, 2013.

[42] NIST. Nitrogen. Last accessed 6 June 2022.

[43] K. Oura, M. Katayama, A. V. Zotov, V. G. Lifshits, and A. A. Saranin. *Surface Science, An Introduction*. Springer Berlin, Heidelberg, 1 edition, 2003.

[44] John P. Perdew, Kieron Burke, and Matthias Ernzerhof. Generalized gradient approximation made simple. *Phys. Rev. Lett.*, 77:3865–3868, Oct 1996.

[45] James P. Sethna. *Statistical Mechanics: Entropy, Order Parameters and Complexity*. Oxford University Press, second edition edition, 2021.

[46] thermal. *Thermal Physics*. thermal, 1.

[47] Jos Thijssen. *Computational Physics*. Cambridge University Press, 2 edition, 2007.

[48] Mark E. Tuckerman. *Statistical Mechanics: Theory and Molecular Simulation*. Oxford University Press Inc., New York, 2010.

[49] Pauli Virtanen, Ralf Gommers, Travis E. Oliphant, Matt Haberland, Tyler Reddy, David Cournapeau, Evgeni Burovski, Pearu Peterson, Warren Weckesser, Jonathan Bright, Stéfan J. van der Walt, Matthew Brett, Joshua Wilson, K. Jarrod Millman, Nikolay Mayorov, Andrew R. J. Nelson, Eric Jones, Robert Kern, Eric Larson, C J Carey, İlhan Polat, Yu Feng, Eric W. Moore, Jake VanderPlas, Denis Laxalde, Josef Perktold, Robert Cimrman, Ian Henriksen, E. A. Quintero, Charles R. Harris, Anne M. Archibald, Antônio H. Ribeiro, Fabian Pedregosa, Paul van Mulbregt, and SciPy 1.0 Contributors. SciPy 1.0: Fundamental Algorithms for Scientific Computing in Python. *Nature Methods*, 17:261–272, 2020.

DEPARTMENT OF SOME SUBJECT OR TECHNOLOGY
CHALMERS UNIVERSITY OF TECHNOLOGY
Gothenburg, Sweden
www.chalmers.se

CHALMERS
UNIVERSITY OF TECHNOLOGY